

We would like to thank all referees and Dr. Yang for their helpful comments and insightful suggestions.

Reply to comments by Anonymous Referee #1

This paper describes atmospheric cycles of sea-salt aerosols in polar regions using model and remote sensing measurement (CALIOP). Authors applied and improve the model, GEOS-chem., to simulate spatial distribution and origins of sea-salt aerosols on basis of various parameters such as salinity of surface snow. They derived an interesting conclusion that sea-salt aerosols in the winter were involved in blowing snow rather than frost flowers on sea-ice. On the whole, the topic of the manuscript is relevant and suitable for the scope of the “Atmospheric Chemistry and Physics. The topics and results deserve to be made available to the scientific community and to be exploited in terms of atmospheric aerosols and ice core community in polar regions. Therefore, this study adds very useful information to our knowledge on the sea-salt cycles involved in blowing snow in polar regions. From this reason, I support publication of this work in ACP. However, the current version contains obvious weaknesses, therefore I recommend a major revision. Details are shown as follows.

1. Size distributions of sea-salt aerosols In the GEOS-Chem. Model, spatial distributions of the concentrations of sea-salt aerosols were calculated on assumption of dry deposition velocity and emission from some origins (e.g., open water, frost flowers, and snow). Sea-salt aerosols were distributed from ultrafine to coarse modes in the polar regions during winter – spring (e.g., Hara et al., ACP, 2011).

Hara, K., et al.: Seasonal features of ultrafine particle volatility in the coastal Antarctic troposphere, *Atmospheric Chemistry and Physics*, doi:10.5194/acp-11-9803-2011, 2011.

What is procedure to calculate and treat size distributions and concentrations of sea- salt aerosols? What are the initial size distributions of particles immediately after emission from sea-ice and ocean? I think that these parameters are probably as same as those in your previous work (Huang and Jaegle, ACP, 2017). If so, add short explanation about processing of aerosol size distribution in the model for readers. If not, details should be mentioned.

Yes, our size distribution assumptions are the same as in Huang and Jaeglé (2017) and we have clarified this in the revised manuscript:

“We use two SSA size bins: accumulation mode ($r_{dry} = 0.01\text{--}0.5 \mu\text{m}$) and coarse mode ($r_{dry} = 0.5\text{--}8 \mu\text{m}$).”

“The size distribution of wind-lifted snow particles follows a two-parameter gamma distribution (Yang et al., 2008 and references therein). Once sublimated, snow particles are released as SSA particles. We assume that 5 SSA particles are produced per snowflake ($N=5$) based on a comparison against observations of submicron SSA mass concentrations at Barrow, Alaska (Huang and Jaegle, 2017). The size distribution of blowing snow SSA is determined from the

size distribution of snow particles, $N (=5)$, and salinity. The resulting emitted mass of blowing snow SSA is obtained by integrating this size distribution into the two SSA size bins.”

“The size distribution of SSA from frost flowers follows a lognormal size distribution with a geometric mean diameter of $0.015 \mu\text{m}$ and a geometric standard deviation of 1.9 (Xu et al., 2013). This size distribution is integrated into the two GEOS-Chem SSA size bins to obtain the emitted mass of SSA from frost flowers.”

2. Dry deposition velocity. In this study, aerosol dry deposition velocity was fixed to 0.03 cm s^{-1} , corresponding to that of particles with size of ca. $2 \mu\text{m}$ in diameter. As shown by Rhodes et al. (2017) and Hara et al. (2017), sea-salt aerosols and ice particles containing sea-salts were released from snow and frost flowers on sea-ice. Then, size of sea-salt particles and ice particles containing sea-salts can be changed through sublimation and efficient dry deposition of larger sea-salt particles in the atmosphere. In general, the coarser aerosols have larger dry deposition velocity (shorter residence time). Therefore, processing of initial size distribution and modification of size distribution involved simultaneously with dry deposition and sublimation is the most important to simulate the concentrations and spatial distribution of sea-salt aerosols. Because aerosol dry deposition velocity has size-dependence, the fixed and assumed aerosol dry deposition velocity can result in mis-estimation. I understand that it is difficult to input all parameters in model calculation. However, sensitivity of dry deposition on the sea-salt concentrations should be checked. Ideally, size dependence of dry deposition velocity is included in the model (I do not require it this time, but I hope it for progress in the future).

Rhodes, R., Yang, X., Wolff, E., McConnell, J. and Frey, M.: Sea ice as a source of sea salt aerosol to Greenland ice cores: a model-based study, *Atmospheric Chemistry and Physics*, 17(15), 9417–9433, doi:10.5194/acp-17-9417-2017, 2017.

Our description of the dry deposition parameterization in GEOS-Chem was unclear and incomplete. The constant 0.03 cm/s dry deposition velocity over snow and ice applies to all aerosols except dust and sea salt. For sea salt in particular, we do assume a size dependent dry deposition velocity. More detail on the sea salt deposition velocity parameterization is now given in the revised manuscript:

“Dry deposition in the GEOS-Chem follows a standard resistance-in-series scheme based on Wesely (1989) as described by Wang et al. (1998). Dry deposition of SSA in the model follows the Zhang et al. (2001) size-dependent scheme over land, and is calculated based on the Slinn and Slinn (1980) deposition model over ocean and sea ice, as implemented by Jaeglé et al. (2011) in GEOS-Chem. The strong size-dependence of SSA deposition is taken into account by integrating the dry deposition velocity over each of the 2 SSA size bins using a bimodal size distribution including growth as a function of local relative humidity (RH). Sedimentation of SSA is calculated throughout the atmospheric column based on the Stokes velocity scheme.”

3. Potential frost flower (PFF) coverage PFF were estimated using air temperature and thickness of sea-ice in the study. Actually, frost flower can be formed on new and young sea-ice. In this study, threshold of newly formed sea-ice thickness is 10 cm . In my experience, this value is

small, because frost flower can be appeared on sea-ice even with thickness of ca. 30cm. If the threshold was smaller, the model results can be underestimated. What is the impact of sea-ice thickness in the model?

The assumed thickness threshold in the model has relatively little impact on our frost flower emissions. Following the suggestion of this reviewer, we conducted a sensitivity study inhibiting the frost flower emission with sea ice thickness over 30cm. We find that frost flower emissions increase by less than 10% over the Arctic, and less than 1% over the Antarctic. This small sensitivity to the assumed the sea ice thickness threshold is a result of the significant decrease in frost flower growth rate with increasing ice thickness (Kaleschke et al., 2004).

Kaleschke, L., Richter, A., Burrows, J., Afe, O., Heygster, G., Notholt, J., Rankin, A. M., Roscoe, H. K., Hollwedel, J., Wagner, T., and Jacobi, H.-W.: Frost flowers on sea ice as a source of sea salt and their influence on tropospheric halogen chemistry, *Geophys. Res. Lett.*, 31, L16114, doi:10.1029/2004GL020655, 2004.

4. Spatial distribution (Figs. 1 and 4) Spatial distribution of aerosol extinction coefficients and model results during cold seasons were depicted in Figs. 1 and 4. These plots provide us very interesting information to understand atmospheric sea-salt cycles in Arctic and Antarctica. However, these periods correspond to develop sea-ice extent, so that these distributions included also seasonal feature of sea-ice extent, which is associated with origins of sea-salt aerosols. Seasonal and spatial variations of source strength and origins of sea-salt aerosols should be taken into account. To exclude influences of the seasonal features, I suggest that the selected months are shown, for example month with maximum of sea-ice extent (March in Arctic and September in Antarctica).

Following the suggestion of this reviewer, we have now added two figures showing monthly mean aerosol extinction coefficients from CALIOP and models during each cold month (November-April in Arctic and May-October in Antarctica) in the Supplementary material (Figures S5 and S6). Overall, the monthly comparisons are consistent with the cold-season comparison, with STD+Opt. Snow best capturing the spatial distributions of CALIOP aerosol extinction coefficients among four model simulations.

Reply to comments by Anonymous Referee #2

This is a well written manuscript describing modeling of Arctic aerosol and comparison of these models to observations from CALIOP satellite lidar observations. The model, GEOS-Chem, uses various parameterizations of aerosol production mechanisms, and addition of a blowing snow mechanism brings the model closer to observations. The blowing snow model is further refined by varying the surface snow salinity to improve agreement with observations. An example of an event of blowing snow is shown.

Overall, I feel that this is a well written manuscript, but that the identification of model modifications with specific physical processes sometimes goes further than is justified and/or alternative hypotheses have not been explored fully. The CALIOP data indicate that there is larger extinction present near the surface than the model would indicate, so a wind speed and snow salinity dependent blowing snow model is added, increasing the modeled aerosol extinction, which brings it closer to observations. However, one needs to consider how definitive the identification of these model variables is with physical processes. Specific questions in this regard are:

1) After adding "blowing snow", the model is tuned to reduce surface snow salinity in MYI areas as compared to FYI areas and over the wintertime season. How robust is the necessity to tune down the salinity? For example, Figure 3 shows distributions of extinction in FYI, MYI, and CAA areas. Visually, I can barely see any difference between the CALIOP observations in panels g, h, and i. Values are about 15 Mm^{-1} from Jan-Apr, low in summer, and increase back to 15 Mm^{-1} towards the end of the year. Is there any statistical difference between these monthly observational distributions? Given the lack of difference between these locations, it seems like the need to optimize the model is weak. Specific monthly values are listed, but it doesn't seem like there is enough information to actually map out this amount of information. For example, could a different single fixed value of salinity be used to optimize the model similarly? It is not unreasonable that surface snow salinity would decrease as you add new snow (which is of low salinity), but the question is how strong the modeling evidence for this decrease is. Please show that the trend from the "optimization" is a real effect larger than statistical errors.

We agree with this reviewer that the need for an optimized time-dependent snow salinity was not very clear in our original manuscript. This was because we made changes with opposing effects partially cancelling each other out, especially for the Arctic: reducing the salinity of MYI and applying a monthly-varying optimized salinity for FYI based on CALIOP extinction observations. As described in the introduction of our manuscript, the lower salinity of MYI and snow on MYI has been clearly demonstrated by observations and is well accepted. In the revised manuscript our STD+Snow simulation now includes this more realistic assumption by lowering the salinity of snow on MYI to 0.01 psu in the Arctic and 0.003 psu in the Antarctic. The new STD+Opt. Snow has the same salinity for MYI as the STD+Snow simulation and uses the fit to CALIOP extinctions to optimize salinity. The impact of the changing snow salinity can be more clearly seen in the revised Figure 3 for FYI (panel g), especially for October-December when the higher salinities on young sea ice (0.36-0.19 psu) lead to a near doubling in aerosol extinction, consistent with CALIOP. We also perform Student's t-test for each cold month and find that significance between these two models' bias are smaller than 0.05 on both FYI and MYI, except

for Antarctic MYI in May, which indicates that STD+Snow and STD+Opt. Snow are statistically significantly different. Applying a single scaling factor for the salinity of surface snow on FYI does not address this model discrepancy over the Arctic. This is now made clearer in the revised manuscript.

“We also examined whether a single fixed value of salinity over FYI can lead to similar improvements in the agreement with CALIOP. The resulting fixed salinities are 0.11 psu over Arctic FYI and 0.018 psu over Antarctic FYI, leading to good overall agreement with CALIOP over the Antarctic (NMB of +5% on FYI and –9% on MYI) with no significant improvement seen in the Arctic (NMB of –7% on FYI and –18% on MYI). We found that over the Arctic, a simulation using a single salinity of 0.11 psu (STD+Const. Snow, Fig. S8g–h) yields results similar to the STD+Snow simulation and cannot explain the high extinction values during fall/early winter. Over Antarctic sea ice, the performance of a simulation with 0.018 psu over FYI shows results similar to the STD+Opt. Snow simulation. Thus there is a stronger case for using a seasonally varying snow salinity over Arctic sea ice than over Antarctic sea ice. We speculate that this might be linked to relatively smaller seasonal variation in sea ice thickness and snow depth for Antarctic sea ice compared to the Arctic. In their snow climatology, Warren et al. (1999) report that the mean snow depth at an Arctic sea ice site increased from 8.7 cm in October to 28.9 cm in March. Satellite-based observations of Arctic FYI thickness show an increase from 0.95 m in October to 2.15 m in May (Kwok and Cunningham, 2015). In contrast, over Antarctic sea ice the mean sea ice thickness and snow depth remained fairly constant during fall–winter (April: 0.48 m for ice thickness and 0.11 m for snow depth; August: 0.52 m for ice thickness and 0.11 m for snow depth) as described in Worby et al. (1998).”

2) Open water areas can produce aerosol directly (by wind blowing over the exposed sea water) or via re-freezing, which might produce frost flowers and/or simply provide a non-snow-covered highly saline surface that snow could blow onto/across. The manuscript does not do justice to hypotheses other than frost flowers. It should leave open the possibility that open water or thin snow cover on ice could be responsible. For instance, the citation below indicates that open water is a source of sea salt aerosol.

May, N. W., P. K. Quinn, S. M. McNamara, and K. A. Pratt (2016), Multiyear study of the dependence of sea salt aerosol on wind speed and sea ice conditions in the coastal Arctic, *J. Geophys. Res. Atmos.*, 121, 9208–9219, doi: 10.1002/2016JD025273.

We now mention this source from leads in the revised manuscript both in the Introduction and in Section 2.3:

“Over polar regions, SSA can also be generated via sublimation of saline blowing snow (Simpson et al., 2007; Yang et al., 2008), wind-blown frost flower crystals (Rankin et al. 2000; Domine et al., 2004; Xu et al. 2013), and by leads in sea ice (Nilsson et al., 2001; May et al, 2016).”

“In this study, we neglect the role of leads as a source of SSA as we found in Huang and Jaeglé (2017) that while this additional source could potentially be important on local scales near leads, overall the regional increase in SSA emissions is less than 10%.”

Another aspect that may affect the ability to model either open water areas or frost flowers is the low spatial resolution (2 x 2.5 degree) of sea ice in the model and also the use of a weekly product (Page 5, line 30) for sea ice concentration. This low time resolution and linear interpolation could affect the ability of the model to represent the small spatial scale (few km) and temporally transient sea ice lead features.

Point well taken. Indeed very small and temporary features such as leads might not be well resolved in the MERRA sea ice fields (based on the 12.5 km resolution observations from the SSM/I instruments on DMSP satellites), which is why we do not consider this source in our manuscript. As noted above, this is now explicitly mentioned in the revised manuscript.

3) The Canadian Archipelago is a region where there is a great deal of land near sea ice. The land can affect the ability of passive microwave satellites to detect sea ice concentrations (called land contamination), and thus could affect the ability to predict frost flower presence. Also, surface winds in the presence of significant topography might not be modeled well at these coarse spatial resolutions. Therefore, I think that there may be a number of factors in this region and caution against overinterpretation. For example, page 9, line 7 indicates a surface snow salinity of 3 psu (nearly 10% of that of sea water) could reconcile differences. Also, it is stated that Alert is near frost-flower producing regions. I think of Alert being in a MYI area, largely surrounded by older sea ice that builds over years. Please cite sources to indicate evidence for Alert (and Neumayer) being in a frost-flower producing area.

The MERRA sea ice component is based on observations from Special Sensor Microwave Imager (SSM/I) instruments on Defense Meteorological Satellite Program (DMSP) satellites, which have a native resolution of 12.5km x 12.5km. The proximity of coastal ocean grid to land, can indeed lead to false ice concentration signals, and the land contamination errors are quantified in Maslanik et al. (1996). The land contamination errors are relatively small in SSM/I, compared to Scanning Multichannel Microwave Radiometer (SSM/R) due to higher resolutions (Maslanik et al., 1996). In addition, land masks are used to alleviate the impact of land contamination (Maslanik et al., 1996). Intercomparison of SSM/I sea ice concentrations with ship-based observations and independent satellite products are discussed in Kaleschke et al. (2001), Kern et al. (2003) and Andersen et al. (2007). Overall, the SSM/I with ARTIST Sea Ice algorithm (ASI) algorithm yields a reasonable representation of sea ice concentrations.

As noted by this reviewer, Alert is in proximity to MYI region. Our frost flower model predicts the most active frost flower emission region to be over the Canadian Arctic Archipelago, and Alert is closest to this region among the three Arctic sites. Therefore, Alert may receive large influence from frost flowers compared to other Arctic sites. We have changed the wording in the revised manuscript to clarify this point.

Andersen, S., Tonboe, R., Kaleschke, L., Heygster, G., and Pedersen, L. T.: Intercomparison of passive microwave sea ice concentration retrievals over the high-concentration Arctic sea ice, *J. Geophys. Res.*, 112, C08004, doi:10.1029/2006JC003543, 2007.

Kaleschke, L., Lüpkes, C., Vihma, T., Haarpaintner, J., Bochert, A., Hartmann, J. and Heygster, G.: SSM/I sea ice remote sensing for mesoscale ocean-atmosphere interaction analysis. *Canadian Journal of Remote Sensing*, 27(5), pp.526-537, 2001.

Kern, S., Kaleschke, L. and Clausi, D.A.: A comparison of two 85-GHz SSM/I ice concentration algorithms with AVHRR and ERS-2 SAR imagery. *IEEE Transactions on Geoscience and Remote Sensing*, 41(10), pp.2294-2306, 2003.

Maslanik, J.A., Serreze, M.C. and Barry, R.G.: Recent decreases in Arctic summer ice cover and linkages to atmospheric circulation anomalies. *Geophysical Research Letters*, 23(13), pp.1677-1680, 1996.

Minor comments:

Page 2, line 20. This sentence is somewhat confusing with respect to what surface is being discussed. Is the top of the newly forming first year ice's salinity being discussed? If so, please clarify that this is the ice surface rather than snow.

Yes, this has been clarified in the revised manuscript.

Page 3, line 3. There is no discussion of open water as a sea salt source.

The role of leads has been included in the introduction of the revised manuscript as part of our response to comment #2.

Page 3, line 27. The wording of "aerosol extinctions and the layers beneath" maybe could be improved.

We have changed the wording in the manuscript.

Page 4, line 20. I think it should be "...with a 1-year..."

This was modified in the revised manuscript.

Page 6, line 26. The wording of "reducing the bias" maybe could be improved (the bias became larger, not smaller, but closer in magnitude to zero).

This has been improved in the manuscript.

Overall, I feel that this manuscript argues well for the need to add a wintertime sea salt aerosol source to the Arctic and this source seems to be effectively modeled by a blowing snow model, but that some further refinements of this model may not be appropriately linked to physical processes (e.g. surface snow salinity changes and frost flowers). Those aspects of the manuscript should be further defended by statistical methods or should be written in a more cautious manner, including alternate hypotheses that seem consistent with the data.

Reply to short comments by Dr. Yang

General comments: This manuscript reports a GEOS-chem model study of sea-ice soured SSA (from both blowing snow and frost flowers) and their impacts on polar aerosol extinction. Numerous model results via changing various parameters are performed and compared to remote sensing (CALIPSO) data. Some results are quite interesting, adding novel information to our knowledge regarding polar SSA production. Authors even derive an ‘optimized’ seasonal trend of snow salinity. Due to the lack of year around blowing snow and snowpack salinity measurements on polar sea ice surface, we almost know nothing about seasonal variation regarding snow salinity. For this reason, I will treat their modelling-based seasonal snow salinity as a weakness. Instead, I think it highlight an issue which is largely unknown to our knowledge. As we know snow salinity is one of the critical factor that could determine both salt mass loading and their airborne budget (via affecting size spectrum and then lifetime). Therefore, it is a quite important to investigate this parameter in a modelling study, though it needs justification as reviewers pointed out. In general, this is well written manuscript with some interesting results presented. It fits well the scope of the ‘Atmospheric Chemistry and Physics’ and will benefit relevant communities in sea ice, ice core and boundary layer chemistry. Thus, I support publication of this work in ACP after a revision (see below my specific comments).

Specific comments: The STD+Snow model run overestimates satellite extinction coefficients. Authors attribute this overestimation to ‘higher’ snow salinity applied in their model. However, I notice that the salinity levels of 0.1 psu for the Arctic and 0.03 psu for the Antarctic sea ice is not ‘very’ high comparing to the observation. For example, the 0.03 psu for the SH is only about half of the ‘median’ surface snow salinity (0.06 psu) and $\sim 1/30$ of the ‘mean’ snow salinity (=0.9 psu) observed in the Weddell Sea SIZ (see information in Rhodes et al. 2017). It seems to me the overestimation of SSA by the model could be related to one ‘missed’ process by the model, namely the negative feedback of sublimated water vapour to the ambient air near surface layer, which prevents further evaporation from suspended blown snow particles in the BS layer [Mann et al. 2000]. Thus, it is likely that model (like GOES-chem) without this process could result in overestimated bulk sublimation and then SSA production. I will not blame them not considering this process in their model, as it is out of the range of this study, but it would be useful if some discussions can be made.

Mann, G. W., Anderson, P. S., and Mobbs, S. D.: Profile measurements of blowing snow at Halley, Antarctica, *J. Geophys. Res.*, 105, 24,491–24,508, 2000.

Another factor that could be responsible for the overestimation may come from one assumption made in this model set-up. According to their previous model study (Huang and Jaegle 2016), they assumed that one wind-blown particles will generate 5 sub- SSA, instead of one as assumed in the original parameterization by Yang et al. (2008). Is this term making some differences? It would be helpful if some discussions can be made as a model sensitivity study.

Yang, X., Pyle, J. A., and Cox, R. A.: Sea salt aerosol production and bromine release: Role of snow on sea ice, *Geophys. Res. Lett.*, 35 (L16815), doi:10.1029/2008gl034536, 2008.

Indeed, our derived seasonal varying surface snow salinity is based on the hypothesis that the discrepancies between CALIOP and the STD+Snow simulation in the magnitude and seasonal cycle of aerosol extinction coefficients are due to our simplifying assumption of a uniform surface snow salinity over sea ice. We cannot rule out the alternative explanations that the overestimate of Antarctic aerosol extinctions is caused by the fact that our simulation does not include the negative feedback of water vapor sublimation or by our assumption of number of particle produced per snowflake (N).

We mention these possibilities in the revised manuscript. To address Dr. Yang's concerns, we have conducted a sensitivity blowing snow simulation assuming N=1. We have included the following discussion in the revised manuscript:

“It is also possible that the discrepancies between observed and modeled aerosol extinction coefficients are due to other factors in the blowing snow parameterization as implemented in GEOS-Chem. For example, our simulation does not include the negative feedback of water vapor sublimation (Mann et al., 2000): as blowing snow particles sublime in unsaturated air, they cause an increase in water vapor and thus cooling of the surrounding air. Both effects lead to an increase in RH near saturation, reducing the sublimation rate. Another underlying assumption is that 5 SSA are produced for each snowflake that sublimates (N=5). We conducted a sensitivity simulation assuming one SSA per snowflake, shown as STD+Snow (N=1) in the supplement (Fig. S7 and S8). This change does not affect the total emissions of blowing snow SSA, but decreases the fraction of SSA in the accumulation mode (see Huang and Jaeglé, 2017). As the extinction efficiency of accumulation mode SSA is larger than that of coarse mode SSA, the assumption of N=1 leads to a 30–50% decrease in modeled extinctions relative to the STD+Snow (N=5) simulation. Overall, this results in improved agreement with CALIOP observations over Antarctic sea ice, but the CALIOP aerosol extinctions are underestimated over the Arctic. Increasing the surface snow salinity over Arctic FYI can address the model discrepancy in aerosol extinction coefficients, but will lead to a factor of 1.5–2 overestimate in SSA mass concentrations.”

Tiny comments: Figure 1, colour bar needs to be improved. It is hard to distinguish the extinguish coefficient values between ~10 and ~20 Mm⁻¹ in the upper panel, and between ~5 and ~10 Mm⁻¹ in the bottom panel of figure 1. A similar problem also appeared in other plots. P10 line 4 and Figure 8: longitude/latitude ranges are mentioned, but not shown in in the corresponding plot. Major longitude/latitude information should be given in all relevant figures.

We have changed the colorbar in Fig. 1 and 4. We have also included the major longitudes and latitude in the relevant figures.

Using CALIOP to constrain blowing snow emissions of sea salt aerosols over Arctic and Antarctic sea ice

Jiayue Huang¹, Lyatt Jaeglé¹, Viral Shah¹

¹Department of Atmospheric Sciences, University of Washington, Seattle, WA

5 Correspondence to: jaegle@uw.edu

Abstract. Sea salt aerosols (SSA) produced on sea ice surfaces by blowing snow events or lifting of frost flower crystals have been suggested as important sources of SSA during winter over polar regions. The magnitude and relative contribution of blowing snow and frost flower SSA sources, however, remain uncertain. In this study, we use 2007–2009 aerosol extinction coefficients from the Cloud-Aerosol Lidar with Orthogonal Polarization (CALIOP) instrument onboard the Cloud-Aerosol
10 Lidar and Infrared Pathfinder Satellite Observation (CALIPSO) satellite and the GEOS-Chem global chemical transport model to constrain sources of SSA over Arctic and Antarctic sea ice. CALIOP retrievals show elevated levels of aerosol extinctions ($10\text{--}20 \text{ Mm}^{-1}$) in the lower troposphere (0–2 km) over polar regions during cold months. The standard GEOS-Chem model underestimates the CALIOP aerosol extinctions by 50–70%. Adding frost flower emissions of SSA fails to explain the CALIOP observations. With blowing snow SSA emissions, the model captures the overall spatial and seasonal variation of
15 CALIOP aerosol extinctions over the polar regions, but ~~overestimates springtime~~underestimates aerosol extinctions over Arctic sea ice in fall–early winter and overestimates winter-spring extinctions over Antarctic sea ice. We ~~reduce~~infer the monthly surface snow salinity ~~over multi~~on first-year sea ice ~~and infer the monthly FYI snow salinity~~ required to minimize the discrepancy between CALIOP extinctions and the GEOS-Chem simulation. The empirically-derived snow salinity shows a decreasing trend ~~in~~ between fall and spring. The optimized blowing snow model with inferred snow salinities generally agrees
20 with CALIOP extinction observations to within 10% over sea ice, but underestimates aerosol extinctions over the regions where frost flowers are expected to have a large influence. Frost flowers could thus contribute indirectly to SSA production by increasing the local surface snow salinity and, therefore, the SSA production from blowing snow. We carry out a case study of an Arctic blowing snow SSA feature predicted by GEOS-Chem and sampled by CALIOP. Using backtrajectories, we link this feature to a blowing snow event which occurred 2 days earlier over first-year sea ice and was also detected by CALIOP.

25 1 Introduction

Sea salt aerosols (SSA) are produced via wave breaking in the open ocean (Lewis and Schwartz, 2004; De Leeuw et al., 2011 and references therein). Over polar regions, SSA can also be generated via sublimation of saline blowing snow (Simpson et al., 2007; Yang et al., 2008) ~~and~~ wind-blown frost flower crystals (Rankin et al. 2000; Domine et al., 2004; Xu et al. 2013) and by leads in sea ice (Nilsson et al., 2001; May et al. 2016). SSA production from blowing snow events requires strong
30 winds ($> 7 \text{ m/s}$) and depends on the salinity of snow cover on sea ice (Yang et al., 2008). Frost flowers grow over new sea ice formed from open leads under low ambient temperature ($< -20^\circ\text{C}$) (Kaleschke et al., 2004). These two sea ice sources of SSA

have been proposed to help explain polar observations of wintertime maxima in SSA mass concentrations (Wagenbach et al., 1998; Weller et al., 2008; Jourdain et al., 2008; Udisti et al., 2012; Huang and Jaeglé, 2017), the depletion of sulfate-to-sodium mass ratio in winter SSA relative to bulk sea water at sites in Antarctica (Wagenbach et al., 1998; Rankin et al., 2000; Jourdain et al., 2008; Hara et al., 2012) and some sites in the Arctic (Jacobi et al., 2012; Seguin et al., 2014), as well as the increase in Na⁺ deposition fluxes during glacial periods relative to interglacial periods (Wolff et al. 2006; Fischer et al., 2007; Abram et al., 2013).

In a previous study (Huang and Jaeglé, 2017), we used the GEOS-Chem chemical transport model to examine the relative roles of blowing snow and frost flowers as sources of polar SSA during winter. Our study was based on the blowing snow parameterization developed by Yang et al. (2008) and the frost flower parameterization of Xu et al. (2013). We compared our simulations to in situ observations of SSA mass concentrations at three surface sites in the Arctic and two sites in coastal Antarctica, showing that blowing snow appeared to be the dominant source of polar SSA during winter. Here, we further constrain the spatial and temporal distribution of polar sources of SSA by using observations of aerosol extinction coefficients from the Cloud-Aerosol Lidar with Orthogonal Polarization (CALIOP) instrument onboard the Cloud-Aerosol Lidar and Infrared Pathfinder Satellite Observations (CALIPSO) satellite together with the GEOS-Chem model.

One of the main uncertainties in estimating blowing snow emissions is the salinity of snow on sea ice. In our previous work (Huang and Jaeglé, 2017), we assumed constant surface snow salinity over Arctic (0.1 practical salinity unit, or psu) and Antarctic (0.03 psu) sea ice. In reality, surface snow salinity is highly variable in time and space. The sources of sea salt in snow over sea ice include upward migration of brine from the sea ice surface, incorporation of frost flowers and SSA deposition from the nearby open ocean (Domine et al., 2004). Initial sea ice formation is accompanied by upward salt transport, such that first-year sea ice (FYI) has a high surface salinity reaching 20–100 psu at the sea ice surface (Weeks and Lee, 1958; Martin, 1979; Weeks and Ackley, 1986). Nakawo and Sinha (1981) found that sea ice salinity decreases rapidly within the first week of sea ice formation in fall, and then decreases more slowly between December and May in the Canadian Arctic. Worby et al. (1998) showed that ice with a thickness of less than 0.05 m displayed salinities of 9–28 psu, while ice thicker than 0.05 m had salinities of 4–8 psu, which decreased linearly with ice thickness. As snow accumulates on FYI throughout winter, the brine is wicked upward resulting in brine-wetted snow (Barber et al., 1995). Snow salinity is highest in the first 10 cm above FYI, with values of 1–20 psu (Geldsetzer et al., 2009) and then decreases rapidly as the snow cover gets thicker, with low salinities on the surface of thick snow (Nandan et al., 2017). Older and thicker multiyear sea ice (MYI), is desalinated by flushing and gravity drainage during repeated summer melt cycles, such that the overlaying snow has very low salinity. Krnavek et al. (2012) reported that surface snow salinity sampled on MYI was 0.01 psu, compared to 0.1 psu for snow on thick FYI and 0.8 psu on recently frozen thin FYI in March near Barrow, Alaska.

The role of frost flowers as a direct source of SSA remains subject to debate. Some studies have shown that strong winds inhibit frost flower formation and bury existing frost flowers with snow (Perovich and Richeter-Menge, 1994; Rankin et al.,

2000), while field experiments show that frost flowers are difficult to break (Domine et al., 2005; Alvarez-Aviles et al., 2008; Obbard et al. 2009). In addition, laboratory experiments show that evaporating frost flowers form a cohesive chunk of salt (Yang et al., 2017), which is unlikely to be a direct source of SSA even when exposed to large wind speeds (Roscoe et al., 2011).

5 In this study, we use 3 years (2007–2009) of CALIOP aerosol extinctions to constrain the spatial and temporal distribution of polar SSA emissions with the GEOS-Chem model. Satellite observations and GEOS-Chem simulations are described in section 2. In section 3, we evaluate the model’s ability to reproduce observed aerosol extinctions over the Arctic and Antarctic sea ice regions with and without sea ice sources of SSA. In section 4, we develop an empirical parameterization of seasonally-varying surface snow salinity on FYI. In section 5, we conduct a case study of an Arctic blowing snow event and the resulting SSA
10 observed by CALIOP.

2 Observations and model simulations

2.1 CALIOP observations of aerosol extinction coefficients

The CALIOP Lidar measures backscatter signals of optical pulses at 532 and 1064 nm (Winker et al., 2009). CALIOP samples the optical properties of clouds and aerosols during daytime and nighttime with a 16-day repeat cycle. It has a sampling
15 resolution of 335 m horizontally and 30 m vertically below 30–40 km altitude. In this study, we use vertical profiles of 532 nm aerosol extinctions from CALIOP Level 2 (L2) version 4.10 profile data for 2007–2009 (Winker, 2016). L2 data is retrieved with a set of algorithms, which identify the cloud and aerosol layers and classify their feature types (Liu et al., 2009). The layer detection algorithm is performed downward for single shots and profiles are averaged horizontally at 1, 5, 20 and 80 km to achieve good signal-to-noise-ratio (SNR) for aerosol retrievals (Winker et al., 2009). The estimated detection sensitivity of the
20 CALIOP 532-nm channel varies with different horizontal averaging, with better sensitivity at larger horizontal averaging (80 km). Nighttime CALIOP extinction coefficients have better sensitivity than daytime observations, which are affected by noise from solar radiation scattering (Winker et al., 2009).

We average monthly CALIOP L2 aerosol extinction profiles poleward of 60° over a 2° latitude by 5° longitude horizontal grid in 60 m vertical bins, using the same approach as Winker et al. (2013). When no aerosols are detected and the layer is classified
25 as “clear air”, we assign it an extinction coefficient value of 0.0 km⁻¹. Following Winker et al. (2013), we exclude the following aerosol layers from our gridded averages: (1) all aerosol layers within 60 m of the surface to avoid surface contamination, (2) layers with a Cloud Aerosol Discrimination (CAD) score falling outside the range of -100 to -20, (3) aerosol layers with
uncertainty flags of 99.9 km⁻¹ ~~when the retrieval is considered failed for aerosol extinctions~~ and the layers beneath, (4) extinction QC flags indicating possible large errors, (5) “clear air” under the lowest detected aerosol layer with base below
30 250 m to avoid low bias for undetected surface-attached aerosol. In addition, we exclude very high values of aerosol extinctions

(> 0.35 km⁻¹) below 2 km poleward of 60° during cold months (September–May for the Arctic and March–November for the Antarctic), as they are likely related to diamond dust misclassified as aerosol (Di Pierro et al., 2013).

The CALIOP nighttime retrievals over polar regions are limited during summer months (May–July in the Arctic, November–January in the Antarctic), with maximum latitudinal extents of 55° latitude beyond which only daytime retrievals are available.

5 Daytime retrievals have higher detection thresholds and can only detect aerosol layers with relatively high extinctions (Fig. S1–2). Therefore, at a given latitude fewer aerosol layers are detected in the daytime retrievals, and the average daytime extinction coefficients are lower than the nighttime ones over polar regions (Fig. S3). Most of our work is based on analysis of nighttime CALIOP retrievals during winter over polar regions. However, to reconstruct the full seasonal cycle of aerosol extinctions over polar regions, we calculate nighttime equivalent aerosol extinction profiles by combining both daytime and
10 nighttime CALIOP extinctions coefficients, following the ~~empirical~~ algorithm ~~derived by~~ described in Di Pierro et al. (2013). This approach provides an empirical correction for the differences in detection sensitivity and aerosol extinctions in the daytime CALIOP retrievals (more details are given in the Supplement).

2.2 The GEOS-Chem chemical transport model

15 We use the GEOS-Chem (v10-01) 3-D global chemical transport model (Bey et al., 2001) driven by meteorological fields from the Modern Era Retrospective-Analysis for Research and Applications (MERRA; Rienecker et al., 2011). The MERRA assimilated meteorological fields have a native horizontal resolution of 0.5° latitude by 0.666° longitude with 72 vertical levels, which we regrid to 2°×2.5° horizontal resolution and 47 vertical levels with merged levels above 80 hPa.

We conduct a three-year (2007–2009) global simulation of tropospheric aerosol-oxidant chemistry. The model is initialized
20 with [a](#) 1-year spin up. Global anthropogenic emissions are from EDGAR v4.2 (Emissions Database for Global Atmospheric Research, Olivier and Berdowski, 2001) for 1970–2008. For the years after 2008, anthropogenic emissions are scaled relative to year 2008, based on government statistics for different countries/regions (van Donkelaar et al., 2008). Over North America, the anthropogenic emissions are from the 2011 National Emissions Inventory (NEI2011; <https://www.epa.gov/air-emissions-inventories/2011-national-emissions-inventory-nei-data>) produced by the US Environmental Protection Agency (EPA), with
25 annual scaling factors from the EPA for other years. Over Asia, the anthropogenic emissions are from the MIX emission inventory (Li et al., 2017). Over Europe, we use the Co-operative programme for monitoring and evaluation of long range transmission of air pollutants in Europe (EMEP) anthropogenic emissions (<http://www.ceip.at/review-of-inventories/>). Monthly biomass burning emissions are from the Global Fire Emissions Database version 4 (GFEDv4, van der Werf et al., 2010). Black carbon (BC) and organic carbon (OC) emissions are based on the Bond et al. (2007) monthly emission inventory,
30 including sources from fossil fuel and biofuel. Dust emissions are based on the dust entrainment and deposition scheme from

Zender et al. (2003). Biogenic emissions of volatile organic compounds (VOCs) are from the Model of Emissions of Gases and Aerosols from Nature version 2.1 (MEGAN 2.1, Guenther et al., 2012). The HO_x-NO_x-VOC-O₃-BrO_x tropospheric chemistry chemical mechanism is described in Mao et al. (2010, 2013) with recent updates in biogenic VOC chemistry (Fisher et al., 2016; Travis et al., 2016). The gas-particle partitioning of SO₄²⁻-NO₃⁻-NH₄⁺ aerosol is computed with the ISORROPIA II thermodynamic module (Fountoukis and Nenes, 2007), as implemented by Pye et al. (2009).

The open-ocean emissions of SSA are a function of wind speed and sea surface temperature (SST) as described in Jaeglé et al. (2011). In Huang and Jaeglé (2017), we inferred that wave-breaking SSA emissions are suppressed during summer at coastal polar sites with cold waters (SST < 5°C). As in Huang and Jaeglé (2017), we reduce SSA emissions for these cold waters. We use two SSA size bins: accumulation mode (r_{dry} = 0.01–0.5 μm) and coarse mode (r_{dry} = 0.5–8 μm).

10 Advection is based on the Lin and Rood (1996) advection algorithm and boundary layer mixing is computed using the non-local scheme in Lin and McElroy (2011). Dry deposition in the GEOS-Chem follows a standard resistance-in-series scheme based on Wesely (1989) as described by Wang et al. (1998). Dry deposition of SSA in the model follows the Zhang et al. (2001) size-dependent scheme over land, and is calculated based on the Slinn and Slinn (1980) deposition model over ocean. ~~The dry deposition velocity for aerosols over snow and ice is assumed to be 0.03 cm s⁻¹ in the model.~~ and sea ice, as implemented by Jaeglé et al. (2011) in GEOS-Chem. The strong size-dependence of SSA deposition is taken into account by integrating the dry deposition velocity over each of the 2 SSA size bins using a bimodal size distribution including growth as a function of local relative humidity (RH). Sedimentation of SSA is calculated throughout the atmospheric column based on the Stokes velocity scheme. Wet deposition of aerosol includes convective updraft, washout and rainout from precipitation (Liu et al., 2001), as well as snow scavenging (Wang et al., 2011).

20 ~~The open-ocean emissions of SSA are a function of wind speed and sea surface temperature (SST) as described in Jaeglé et al. (2011). In Huang and Jaeglé (2017), we inferred that wave-breaking SSA emissions are suppressed during summer at coastal polar sites with cold waters (SST < 5°C). As in Huang and Jaeglé (2017), we reduce SSA emissions for these cold waters.~~

~~The implementation of blowing snow and frost flower SSA emissions in GEOS-Chem is described in detail in Huang and Jaeglé (2017). Briefly, the blowing snow parameterization follows based on the parameterizations of Yang et al. (2008). We assume a uniform surface, 2010 as implemented by Huang and Jaeglé (2017). The SSA production from blowing snow is a function of RH, temperature, age of snow, snow salinity, and wind speed. The size distribution of 0.1 psu over Arctic sea ice based on wind-lifted observations of surface snow salinity (Mundy et al., 2005; Krnavek et al., 2012). Over Antarctic sea ice, we assume 0.03 psu for surface snow as more frequent snowfall likely dilutes the salinity. particles follows a two-parameter gamma distribution (Yang et al., 2008). We calculate a mean and references therein). Once sublimated, snow age of 3 days for the Arctic and 1.5 days for the Antarctic from MERRA. In addition, we particles are released as SSA particles. We assume that~~

25 assume a uniform surface, 2010 as implemented by Huang and Jaeglé (2017). The SSA production from blowing snow is a function of RH, temperature, age of snow, snow salinity, and wind speed. The size distribution of 0.1 psu over Arctic sea ice based on wind-lifted observations of surface snow salinity (Mundy et al., 2005; Krnavek et al., 2012). Over Antarctic sea ice, we assume 0.03 psu for surface snow as more frequent snowfall likely dilutes the salinity. particles follows a two-parameter gamma distribution (Yang et al., 2008). We calculate a mean and references therein). Once sublimated, snow age of 3 days for the Arctic and 1.5 days for the Antarctic from MERRA. In addition, we particles are released as SSA particles. We assume that

30 5 SSA particles are produced per snowflake (N=5) based on a comparison against observations of submicron SSA mass

concentrations at Barrow, Alaska (Huang and Jaeglé, 2017). The size distribution of blowing snow SSA is determined from the size distribution of snow particles, $N (=5)$, and salinity. The resulting emitted mass of blowing snow SSA is obtained by integrating this size distribution into the two SSA size bins. In our previous work, we had assumed a uniform salinity on Arctic (0.1 psu) and Antarctic sea ice (0.03 psu) based on mean observations of surface snow salinity (Mundy et al., 2005; Krnavek et al., 2012). Here we use these salinities for FYI, but now take into account the lower surface snow salinity of older sea ice, by assuming that MYI snow salinity is 10 times lower than on FYI (Krnavek et al., 2012): 0.01 psu on Arctic MYI snow and 0.003 psu on Antarctic MYI snow. We calculate a mean snow age of 3 days for the Arctic and 1.5 days for the Antarctic from MERRA.

Frost flower SSA emissions follows the emission scheme of Xu et al. (2013), which follows the empirical wind-dependence of Shaw et al. (2010) and the potential frost flower (PFF) coverage of Kaleschke et al. (2004). The PFF is a function of ambient air temperature, and frost flowers are formed on very new and young sea ice once the ambient air temperature is cold enough ($< \text{about } -20^{\circ}\text{C}$). We set a threshold of 10 cm for the thickness of newly formed sea ice beyond which we assume that frost flowers do not form due to inefficient brine transport through thicker sea ice. The size distribution of SSA from frost flowers follows a lognormal size distribution with a geometric mean diameter of $0.015 \mu\text{m}$ and a geometric standard deviation of 1.9 (Xu et al., 2013). This size distribution is integrated into the two GEOS-Chem SSA size bins to obtain the emitted mass of SSA from frost flowers.

The sea ice concentration boundary conditions in MERRA are derived from the weekly product of Reynolds et al. (2002), which is based on Special Sensor Microwave Imager (SSM/I) instruments on Defense Meteorological Satellite Program (DMSP) satellites. The weekly products have an original spatial resolution of $1^{\circ} \times 1^{\circ}$, and are linearly interpolated in time to each model time step. For each year, we use the preceding summertime minimum sea ice extent in MERRA (September in the Arctic and February in the Antarctic) to infer the location of MYI. FYI extent is calculated by subtracting MYI extent from total sea ice extent (Fig. S4).

In this study, we neglect the role of leads as a source of SSA as we found in Huang and Jaeglé (2017) that while this additional source could potentially be important on local scales near leads, overall the regional increase in SSA emissions is less than 10%.

Our standard simulation (STD) includes tropospheric aerosol-oxidant chemistry and SSA emissions from the open ocean. The STD+Snow simulation is the STD simulation to which we add SSA emissions from blowing snow as in Huang and Jaeglé (2017), with ~~uniform~~ surface snow salinities as described above (0.1 psu on FYI and 0.01 psu on MYI over the Arctic, and 0.03 psu on FYI and 0.03 psu on MYI over the Antarctic). The STD+FF simulation is the STD simulation with SSA emissions from frost flowers. In Section 4, we develop an optimized blowing snow simulation (STD+Opt. Snow), with seasonally varying snow salinity on FYI.

The GEOS-Chem simulations are sampled at the time and location of the CALIOP overpasses and averaged over the same horizontal and vertical grid. For comparison to CALIOP observations, we apply the CALIOP nighttime detection threshold to the model, setting the modeled backscatter coefficients to $0 \text{ Mm}^{-1} \text{ sr}^{-1}$ for backscatter values lower than $0.2 \text{ Mm}^{-1} \text{ sr}^{-1}$.

3 Model evaluation with CALIOP observations

5 3.1 Arctic

The Arctic cold season (November–April) CALIOP extinction coefficients in the lower troposphere (0–2 km above sea level, asl) display values of $10\text{--}30 \text{ Mm}^{-1}$ (Fig. 1a). The largest extinction coefficients occur over the open-ocean regions of the Greenland and Barents Seas. In addition, significant aerosol extinction coefficients ($10\text{--}20 \text{ Mm}^{-1}$) are seen over the sea ice covered Chukchi Sea, East Siberian Ocean, Laptev Sea, Kara Sea and Canadian Arctic Archipelago (Fig. 1a). While the STD
10 GEOS-Chem simulation reproduces the pattern of extinctions over the open ocean regions, it fails to capture the enhancements over sea ice, underestimating aerosol extinction coefficients by $\sim 10 \text{ Mm}^{-1}$ over the central Arctic (Fig. 1b). The normalized mean bias ($\text{NMB} = 100 \times (\overline{\text{Model}} / \overline{\text{Obs}} - 1)$, with $\overline{\text{Model}}$ and $\overline{\text{Obs}}$ representing mean observed and modeled values) is -55% over FYI, and -68% over MYI (Fig. 2a). GEOS-Chem also underestimates CALIOP aerosol extinctions over Northern Russia, which could be due to missing sources of aerosols and their precursors from gas flaring in the region (Li et al., 2016; Klimont
15 et al., 2017; Xu et al., 2017).

In the STD simulation, aerosol extinction coefficients during the cold season are dominated by SSA over the high latitude open ocean and by long-range transport of sulfate aerosols over sea ice (Fig. 1f and g). Adding blowing snow emissions of SSA increases the simulated aerosol extinctions by $\sim 10 \text{ Mm}^{-1}$ over the central Arctic, bringing the STD+Snow simulation in better
20 agreement with CALIOP observations (Fig. 1c and h) ~~and reducing the~~, with a model bias ~~to +16–18%~~ of -7% on FYI and -17% on MYI (Fig. 2b). Inclusion of frost flower emissions of SSA in the STD+FF simulation has the largest influence over Canadian Arctic Archipelago where cold ~~temperature~~ temperatures and open leads co-exist (Fig. 1j), but the overall magnitude of the increase cannot explain the CALIOP extinctions. Monthly maps of the comparison between CALIOP and GEOS-Chem simulations are included in supplement (Fig. S5).

25 Figure 3 compares the vertical and seasonal distribution of aerosol extinction coefficients in the lower troposphere (0–2 km altitude) over FYI, MYI, and the Canadian Arctic Archipelago, where frost flowers are expected to have their largest influence (Huang and Jaeglé, 2017). Over all three regions, the STD simulation underestimates cold season CALIOP extinctions by factors of 3–6 (Fig. 3d and f). The STD+FF simulation reduces the negative model bias, but the modeled extinctions remain
30 too low by 20–40% (Fig. 3d–f). Furthermore, the STD+FF simulation does not capture the rapid increase in CALIOP extinctions in October–December (Fig. 3g–i). We find that applying a single scaling factor to the frost flower emissions cannot address the seasonally-varying model discrepancy. In comparison, the STD+Snow simulation displays the best agreement with

the CALIOP observations, reproducing both the vertical profile and seasonal cycle of CALIOP extinctions. The STD+Snow simulation, however, ~~overestimates~~underestimates the CALIOP aerosol extinctions in October–December by 30–50% (Fig. 3g and f), and underestimates the surface CALIOP cold season aerosol extinctions by up to ~~85~~5 Mm^{-1} ~~below 1 km altitude~~ (Fig. 3d and e). In addition, it predicts a maximum in aerosol extinction during April, while CALIOP observations display their largest concentrations in January–March for FYI, and in March over MYI.

3.2 Antarctic

During the Austral cold season (May–October), CALIOP aerosol extinction coefficients decrease with increasing latitudes, ranging from 20–30 Mm^{-1} at 60°S to 5–10 Mm^{-1} near coastal Antarctica (Fig. 4a). Over Antarctic FYI (Fig. 5a), CALIOP aerosol extinctions display values of 10–14 Mm^{-1} in July–October in the lower troposphere (Fig. 5g), with aerosol extinctions attaining 30 Mm^{-1} near the surface (Fig. 5d). Over MYI sea ice offshore of the Ronne ice-shelf, the CALIOP extinctions are somewhat smaller, reaching 20 Mm^{-1} near the surface (Fig. 5e).

Poleward of 70°S, open ocean SSA dominate aerosol extinction coefficients in the STD simulation (Fig. 4f), accounting for 80% of the extinction, with the remaining 20% due to the combined contributions from sulfate, black carbon and organic aerosols. The STD simulation underestimates CALIOP observations by 5–10 Mm^{-1} (Fig. 5g–i), with a –53% bias over FYI and a –64% bias over MYI (Fig. 2d). The inclusion of frost flowers in the STD+FF simulation leads to a ~ 2 Mm^{-1} increase in extinction coefficients near the Ross and Ronne Ice-shelves where cold temperatures and open leads persist (Fig. 4i). This increase is insufficient to explain CALIOP observations (Fig. 4e and 5).

The STD+Snow simulation increases aerosol extinction coefficients by 10–20 Mm^{-1} in the Indian Ocean (0–100°) and Pacific Ocean (180–270°) sectors (Fig. 4g), where strong winds persist. ~~The~~We find that the inclusion of blowing snow SSA emissions results in a ~~53~~43% overestimate of CALIOP extinctions over FYI sea ice (Fig. 2e) and too strong a seasonal increase in extinctions between May and October (Fig. 5g). Over the smaller MYI region, the positive bias of the STD+Snow simulation is ~~+39~~26% (Fig. 2e, 5e and h). Monthly maps comparing CALIOP and GEOS-Chem are included in supplement (Fig. S6).

4 Blowing snow simulation with optimized snow salinity

While the inclusion of blowing snow leads to improved agreement with CALIOP, we hypothesize that the remaining discrepancies in the magnitude and seasonal cycle of aerosol extinction coefficients are due to our simplifying assumption of a uniform surface snow salinity over ~~sea ice~~FYI.

As discussed in Section 1, the surface snow salinity is highest over thin FYI with little snow cover early in the cold season, declining in the ensuing months as a result of thickening sea ice and increasing snowpack cover (Barber et al., 1995; Kravek

et al., 2012; Weeks and Lee, 1958; Weeks and Ackley, 1986; Nakawo and Sinha, 1981). ~~In addition, snow salinity is very low over MYI as a result of repeated summer melt drainage of brine from the sea ice (e.g., Martin, 1979).~~

As no systematic observations of surface snow salinity are available over sea ice, our approach is to find the monthly salinity of snow on FYI required to minimize the discrepancy between CALIOP extinctions and the GEOS-Chem simulation. ~~For Arctic MYI, we assume a low salinity of 0.01 psu based on observations of Krnavek et al. (2012). Over Antarctic MYI we assume a salinity of 0.003 psu, assuming that frequent snowfall further dilutes the snow salinity.~~ The salinity of surface snow on MYI is the same as in the STD+Snow simulation.

By using a linear regression between the GEOS-Chem simulation and CALIOP monthly extinctions over Arctic sea ice, we derive a surface snow salinity on FYI of 0.9 psu in September, decreasing to 0.09 psu in April (with values of 0.36, 0.26, 0.19, 0.16, 0.16, and 0.14, between October and March). The inferred snow salinities decrease with time and are generally consistent with observations near Alaska reported by Krnavek et al. (2012): 0.8 psu for snow over recently frozen thin FYI and 0.1 psu over thick FYI. For Antarctic FYI, we infer snow salinities of 0.05 psu in April, 0.02 in May–June and 0.018 in July–September. For the rest of the year the salinity is 0.015 psu. These decreasing trends in salinity between fall and spring are consistent with expectations based on the seasonal evolution of FYI thickness, sea ice surface salinity and deepening snow cover (Worby et al., 1998; Warren et al., 1999; Massom et al., 2001; Kwok and Cunningham, 2015).

We use ~~these~~our empirically-derived monthly snow salinities to conduct an optimized blowing snow simulation (STD+Opt. Snow). Over Arctic FYI, the model bias ~~decreases~~changes from ~~+16–7%~~ (STD+Snow) to +8% (STD+Opt. Snow), and for MYI the ~~positive model~~ bias of ~~+18% decreases~~ –17% changes to –2% (Fig. 2b and c). Over Antarctic FYI, the model overestimate decreases from ~~+53–43%~~ (STD+Snow) to +4% (STD+Opt. Snow). Similarly, the model bias over MYI decreases to –10% (Fig. 2e and f). The STD+Opt. Snow simulation displays cold season extinction profiles that are within 5–10% of CALIOP observations over sea ice (Fig. 3d–e and 5d–e). The seasonal cycles are in better agreement with observations ~~(Fig. 3g–h and 5g–h). The, especially in the Arctic for October–December when the inferred FYI salinities (0.36–0.19 psu compared to 0.1 psu in the STD+Opt. Snow simulation shows improved)~~ lead to a near doubling of aerosol extinction (Fig. 3g–h). Over Antarctica, the amplitude of the seasonal cycle of aerosol extinction over FYI is reduced, in better agreement with ~~the~~ CALIOP observations ~~over the Beaufort Sea, due to a reduced contribution from blowing snow emissions for MYI (Fig. 4d5g–h).~~

~~The low snow salinity over MYI, however, leads to an underestimate of aerosol extinctions over the Canadian Arctic Archipelago (Fig. 4d5g–h).~~ We also examined whether a single fixed value of salinity over FYI can lead to similar improvements in the agreement with CALIOP. The resulting fixed salinities are 0.11 psu over Arctic FYI and 0.018 psu over Antarctic FYI, leading to good overall agreement with CALIOP over the Antarctic (NMB of +5% on FYI and –9% on MYI) with no significant improvement seen in the Arctic (NMB of –7% on FYI and –18% on MYI). We found that over the Arctic, a simulation using a single salinity of 0.11 psu (STD+Const. Snow, Fig. S8g–h) yields results similar to the STD+Snow simulation and cannot

explain the high extinction values during fall/early winter. Over Antarctic sea ice, the performance of a simulation with 0.018 psu over FYI shows results similar to the STD+Opt. Snow simulation. Thus there is a stronger case for using a seasonally varying snow salinity over Arctic sea ice than over Antarctic sea ice. We speculate that this might be linked to relatively smaller seasonal variation in sea ice thickness and snow depth for Antarctic sea ice compared to the Arctic. In their snow climatology, Warren et al. (1999) report that the mean snow depth at an Arctic sea ice site increased from 8.7 cm in October to 28.9 cm in March. Satellite-based observations of Arctic FYI thickness show an increase from 0.95 m in October to 2.15 m in May (Kwok and Cunningham, 2015). In contrast, over Antarctic sea ice the mean sea ice thickness and snow depth remained fairly constant during fall–winter (April: 0.48 m for ice thickness and 0.11 m for snow depth; August: 0.52 m for ice thickness and 0.11 m for snow depth) as described in Worby et al. (1998).

Both STD+Snow and STD+Opt. Snow models underestimate CALIOP aerosol extinctions over the Canadian Arctic Archipelago (Fig. 3f). Combining the STD+Opt. Snow and frost flower emissions could help improve the agreement in that region, but it would also lead to substantial overestimates over FYI and MYI for the rest of the Arctic. One possibility is that snow-covered frost flowers in the Canadian Archipelago increase the local surface snow salinity (Domine et al., 2004). The recent study of Hara et al. (2017) in northwestern Greenland proposed that snowfall buries frost flowers and the associated slush layer on new FYI. The resulting brine migrates vertically enriching the surface snow layer, which can be mobilized under strong winds. We estimate that increasing the salinity of snow over the Canadian Archipelago to a value of 3 psu would help reconcile the optimized blowing snow simulation with CALIOP observations. Direct measurements of snow salinity in this region would help confirm this estimate. Similarly, we find that increasing the snow salinity near the Ross ice-shelf region, where frost flowers are expected to occur, would improve the agreement with CALIOP observations.

Figure 6 evaluates the performance of the STD+Opt. Snow simulation against independent observations of SSA mass concentrations at Barrow, Alaska (71.3°N, 156.6°W); Alert, Nunavut, Canada (82.5°N, 62.5°W); Zeppelin, Svalbard (78.9°N, 11.9°E); Neumayer, Antarctica (70.7°S, 8.3°W) and Dumont d'Urville, Antarctica (66.7°S, 140°E). Descriptions of the in situ observations are provided in Huang and Jaeglé (2017). At Barrow, the optimized simulation improves the agreement with observed SSA mass concentrations in November–May. In particular, the enhanced salinity in October–November brings the model closer to the observations. At Zeppelin and Dumont d'Urville, the model bias in the STD+Opt. Snow simulation is reduced relative to the STD+Snow simulation. However, the model bias worsens at Neumayer (STD+Snow: ~~+1~~25%, STD+Opt. Snow: ~~-48~~4%), and the magnitude of model bias remains large at Alert (STD+Snow: ~~+24~~50%, STD+Opt. Snow: ~~-32~~3%). As Neumayer and Alert are close to the frost flower producing regions, compared to other polar sites, this underestimate may be related to an underestimate in the snow salinity in those regions.

It is also possible that the discrepancies between observed and modeled aerosol extinction coefficients are due to other factors in the blowing snow parameterization as implemented in GEOS-Chem. For example, our simulation does not include the negative feedback of water vapor sublimation (Mann et al., 2000): as blowing snow particles sublime in unsaturated air, they

cause an increase in water vapor and thus cooling of the surrounding air. Both effects lead to an increase in RH near saturation, reducing the sublimation rate. Another underlying assumption is that 5 SSA are produced for each snowflake that sublimates (N=5). We conducted a sensitivity simulation assuming one SSA per snowflake, shown as STD+Snow (N=1) in the supplement (Fig. S7 and S8). This change does not affect the total emissions of blowing snow SSA, but decreases the fraction of SSA in the accumulation mode (see Huang and Jaeglé, 2017). As the extinction efficiency of accumulation mode SSA is larger than that of coarse mode SSA, the assumption of N=1 leads to a 30–50% decrease in modeled extinctions relative to the STD+Snow (N=5) simulation. Overall, this results in improved agreement with CALIOP observations over Antarctic sea ice, but the CALIOP aerosol extinctions are underestimated over the Arctic. Increasing the surface snow salinity over Arctic FYI can address the model discrepancy in aerosol extinction coefficients, but will lead to a factor of 1.5–2 overestimate in SSA mass concentrations.

5 A case study of a blowing snow event over the Arctic

Figure 7 shows a case study of a blowing snow SSA event, which occurred on November 6, 2008 over the Arctic. The STD+Snow and STD+Opt. Snow simulations show enhanced extinction coefficients ($40\text{--}80\text{ Mm}^{-1}$) over the Barents Sea along the 60°E longitude line extending from the North Pole to 70°N (Fig. 7b and c). This feature is due to blowing snow SSA and it is not seen in the STD simulation (Fig. 7a) or the frost flower simulation (not shown).

The CALIPSO 00:58–01:12 UTC overpass on November 6, 2008 transected this feature, with CALIOP aerosol extinction coefficients of $50\text{--}150\text{ Mm}^{-1}$ between points A (78°N ; 52.5°E) and B (82°N ; 110°E) labelled in Fig. 7a–c. The cross section along the CALIOP overpass shows that the large extinctions are confined between the surface and 1–2 km altitude (Fig. 7e). This overpass region is mostly covered by FYI (Fig. 7d). We sampled the GEOS-Chem simulations along the same cross section, finding a very good correspondence between the spatial extent of the feature observed by CALIOP and simulated by the STD+Snow and STD+Opt. Snow simulations (Fig. 7g–i). The optimized blowing snow model simulates slightly higher aerosol extinctions due to larger surface snow salinity on FYI in November, and is in better agreement with the 0–2 km CALIOP mean aerosol extinction coefficients (Fig. 7i).

We use the FLEXPART particle dispersion model (Stohl et al., 1998, 2005; Seibert and Frank, 2004) with meteorological data from ERA-Interim with a horizontal resolution of 0.5° to track the origin of this feature. We release 100,000 particles between points A and B at 0.01–2km and track them back in time over 2 days. Figure 8a shows that the air along the AB transect originated in Fig. 7 originates from the $120\text{--}140^\circ\text{E}$ sector at $60\text{--}90^\circ\text{N}$ near the surface (0–100 m), on November 4, 2008 (Fig. 8a). This region is covered by both MYI and FYI (Fig. 7d). The STD+Snow model predicts enhanced blowing snow emissions in this region on November 4, 2008 (Fig. 8b). The CD transect in Fig. 8b shows the CALIOP overpass at 01:11–01:24 UTC November 4, 2008. This CALIOP overpass across this area on that day transect displays elevated 532 nm attenuated

perpendicular backscatter and depolarization ratio below 200 m (Fig. 8c and d), which are co-located with strong surface winds ($>5 \text{ m s}^{-1}$). The pattern of elevated backscatter, surface winds and depolarization ratio satisfies the requirements of the CALIOP blowing snow detection algorithm described in Palm et al. (2011, 2017), who defined blowing snow events as layers with high color ratio (>1), high depolarization ratio (>0.25), strong surface winds ($>4 \text{ m s}^{-1}$), and enhanced backscatter signals below 300 m (ranging between $2.5 \times 10^{-2} \text{ km}^{-1} \text{ sr}^{-1}$ and $0.2 \text{ km}^{-1} \text{ sr}^{-1}$). ~~The~~ Therefore, the FLEXPART-predicted source region and CALIOP blowing snow feature are co-located with enhanced blowing snow emissions in the ~~STD+Snow~~ GEOS-Chem simulation (Fig. 8b). This case study thus shows that CALIOP can detect not only the blowing snow event (Palm et al., 2011) but also the resulting SSA produced after sublimation.

6 Discussion and conclusions

10 In this work, we used the GEOS-Chem chemical transport model to assess the ability of the CALIOP Lidar onboard the CALIPSO satellite to provide constraints on sea ice sources of SSA. We find that mean CALIOP aerosol extinction coefficients below 2 km altitude reach $10\text{--}15 \text{ Mm}^{-1}$ over sea ice covered regions during the 6-month polar cold season. The enhanced extinctions are located below 2 km, with the largest values ($20\text{--}35 \text{ Mm}^{-1}$) occurring near the surface. We find that a standard GEOS-Chem simulation without sea ice sources of SSA underestimates CALIOP extinctions by $50\text{--}70\%$ over Arctic and 15 Antarctic sea ice. A simulation with frost flower SSA emissions is unable to explain the spatial and temporal distribution of CALIOP aerosol extinctions. Adding a blowing snow SSA source results in improved agreement over the Arctic (NMB = $+16\text{--}7\%$ for first year sea ice (FYI) and $+18\text{--}17\%$ over multi-year sea ice (MYI)), but yields a ~~50~~ 43% overestimate of CALIOP extinctions over Antarctic sea ice. Additionally, the simulation including blowing snow SSA tends to ~~overestimate~~ underestimate CALIOP observations ~~towards the end of the cold season (April–May~~ during fall–early winter ~~(October–December~~ over the Arctic and September–October April over the Antarctic).

We hypothesize that our assumption of constant surface snow salinity on FYI (0.1 psu over the Arctic and 0.03 psu over the Antarctic) in the blowing snow simulation could explain this ~~overestimate~~ underestimates. Given the paucity of snow salinity observations, we infer the monthly ~~FYI~~ surface snow salinity on FYI required to minimize the discrepancy between CALIOP extinctions and the GEOS-Chem simulation. The resulting snow salinities decrease progressively between the beginning and 25 end of the cold season (from 0.9 to 0.09 psu for Arctic FYI; 0.05 to 0.018 psu over Antarctic FYI). This decrease is consistent with the seasonally increasing sea ice thickness and accumulating snow depth. ~~We also prescribe a 0.01 psu snow salinity on Arctic MYI and 0.003 psu snow salinity on Antarctic MYI.~~ The optimized blowing snow model using the monthly-varying snow salinities shows improved agreement with CALIOP observations and in situ observations of SSA mass concentrations at five surface sites. However, the optimized blowing snow model tends to underestimate the aerosol extinctions over the 30 Canadian Arctic Archipelago and off the Ross Ice-shelf. Both regions are predicted to favor frost flower growth, which could locally increase the salinity of snow when frost flowers are buried under snow. We find that increasing the Canadian Arctic

Archipelago FYI snow salinity to 3 psu would help reconcile our simulation with CALIOP and in situ observations. Our work, however, cannot rule out other alternative factors contributing to the discrepancy between modeled and observed aerosol extinctions, such as the impact of the negative feedback of water vapor sublimation and our assumption of the number of particle produced per snowflake. Systematic observations of surface snow salinity over multiple sea ice locations and times would help further constrain snow salinities in the Arctic and Antarctic. Furthermore, more extensive observations of sea salt aerosol size distributions during blowing snow events, can help further refine and constraint these assumptions.

We conduct a case study of a blowing snow SSA event over the Arctic which was detected by CALIOP on November 6, 2008 and predicted by our blowing snow simulation. Using FLEXPART, we find that the observed aerosol extinction layer originated 2 days earlier over sea ice below 100m altitude. We demonstrate that CALIOP detects this blowing snow event with enhanced extinction below 200 m and large depolarization ratio, co-located with surface high winds.

Our work suggests that blowing snow emissions are the dominant source of SSA over sea ice covered regions during cold months. As SSA can act as a source of halogens, inclusion of blowing snow in chemical transport models is important to understand springtime bromine explosions and the resulting ozone and mercury depletion events (Schroeder et al., 1998; Simpson et al., 2007; Steffen et al., 2008; Gilman et al., 2010; Yang et al., 2010). Furthermore, these sea-ice sources of SSA can act as ice nuclei for cloud formation, and may increase the downward longwave radiative forcing (Xu et al., 2013). Arctic sea ice has been rapidly changing over the past 30 years, with decreasing sea ice extent and thickness (e.g. Kwok and Rothrock, 2009), a shift towards less MYI and more FYI (Fowler et al., 2004; Maslanik et al., 2007), and a thinning of snow depth in spring (Renner et al., 2014; Blanchard-Wrigglesworth et al., 2015). All these factors are likely to have resulted in an increase in snow salinity on sea ice, and hence increasing SSA emissions from blowing snow. In the Southern Hemisphere, sea ice extent is FYI-dominant, and its annual/seasonal trend is more complex, varying in space. Sea ice extent has been increasing over the Ross Sea, but decreasing over the Amundsen-Bellingshausen Sea over the past decades (Turner et al., 2009; Parkinson and Cavalieri, 2012; Stammerjohn et al., 2012). Consequently, this may have resulted in a shift in the spatial pattern of blowing snow SSA emissions, with increased influence over the Ross Sea and reduced influence over the Amundsen-Bellingshausen Sea.

25 Acknowledgements.

This work was supported by funding from the NASA Atmospheric Composition Modeling and Analysis Program under award NNX15AE32G. The CALIOP data was obtained from the NASA Langley Research Center Atmospheric Science Data Center.

References

- Abram, N. J., Wolff, E. W., and Curran, M. A. J.: A review of sea ice proxy information from polar ice cores, *Quaternary Sci. Rev.*, 79, 168–183, doi:10.1016/j.quascirev.2013.01.011, 2013.
- Alvarez-Aviles, L., Simpson, W. R., Douglas, T. A., Sturm, M., Perovich, D., and Domine, F.: Frost flower chemical composition during growth and its implications for aerosol production and bromine activation, *J. Geophys. Res.*, 113, D21304, doi:10.1029/2008JD010277, 2008.
- Barber, D. G., Reddan, S. P., and Ledrew, E. F.: Statistical Characterization of the Geophysical and Electrical-Properties of Snow on Landfast First-Year Sea-Ice, *J. Geophys. Res.-Oceans*, 100, 2673–2686, doi:10.1029/94jc02200, 1995.
- Bey, I., Jacob, D. J., Yantosca, R. M., Logan, J. A., Field, B. D., Fiore, A. M., Li, Q., Liu, H. Y., Mickley, L. J., and Schultz, M. G.: Global modeling of tropospheric chemistry with assimilated meteorology: Model description and evaluation, *J. Geophys. Res.-Atmos.*, 106, 23073–23095, doi:10.1029/2001jd000807, 2001.
- Blanchard-Wrigglesworth, E., Farrell, S.L., Newman, T. and Bitz, C.M.: Snow cover on Arctic sea ice in observations and an Earth System Model. *Geo. Res. Lett.*, 42(23), 10,342–10,348, doi:10.1002/2015GL066049, 2015.
- Bond, T. C., Bhardwaj, E., Dong, R., Jogani, R., Jung, S. K., Roden, C., Streets, D. G., and Trautmann, N. M.: Historical emissions of black and organic carbon aerosol from energy-related combustion, 1850–2000, *Global Biogeochem. Cy.*, 21, GB2018, doi:10.1029/2006gb002840, 2007.
- de Leeuw, G., Andreas, E. L., Anguelova, M. D., Fairall, C. W., Lewis, E. R., O’Dowd, C., Schulz, M., and Schwartz, S. E.: Production flux of sea-spray aerosol, *Rev. Geophys.*, 49, RG2001, doi:10.1029/2010RG000349, 2011.
- Di Pierro, M., Jaeglé, L., Eloranta, E. W., and Sharma, S.: Spatial and seasonal distribution of Arctic aerosols observed by the CALIOP satellite instrument (2006–2012), *Atmos. Chem. Phys.*, 13, 7075–7095, doi:10.5194/acp-13-7075-2013, 2013.
- Domine, F., Sparapani, R., Ianniello, A., and Beine, H. J.: The origin of sea salt in snow on Arctic sea ice and in coastal regions, *Atmos. Chem. Phys.*, 4, 2259–2271, doi:10.5194/acp-4-2259-2004, 2004.
- Domine, F., Taillandier, A. S., Simpson, W. R., and Severin, K.: Specific surface area, density and microstructure of frost flowers, *Geophys. Res. Lett.*, 32, L13502, doi:10.1029/2005GL023245, 2005.
- Fischer, H., Siggaard-Andersen, M.L., Ruth, U., Röthlisberger, R., and Wolff, E.: Glacial/interglacial changes in mineral dust and sea-salt records in polar ice cores: Sources, transport, and deposition, *Rev. Geophys.*, 45, RG1002, doi:10.1029/2005rg000192, 2007.
- Fisher, J. A., Jacob, D. J., Travis, K. R., Kim, P. S., Marais, E. A., Chan Miller, C., Yu, K., Zhu, L., Yantosca, R. M., Sulprizio, M. P., Mao, J., Wennberg, P. O., Crouse, J. D., Teng, A. P., Nguyen, T. B., St. Clair, J. M., Cohen, R. C., Romer, P., Nault, B. A., Wooldridge, P. J., Jimenez, J. L., Campuzano-Jost, P., Day, D. A., Hu, W., Shepson, P. B., Xiong, F., Blake, D.

- R., Goldstein, A. H., Misztal, P. K., Hanisco, T. F., Wolfe, G. M., Ryerson, T. B., Wisthaler, A., and Mikoviny, T.: Organic nitrate chemistry and its implications for nitrogen budgets in an isoprene- and monoterpene-rich atmosphere: constraints from aircraft (SEAC4RS) and ground-based (SOAS) observations in the Southeast US, *Atmos. Chem. Phys.*, 16, 5969–5991, doi:10.5194/acp-16-5969-2016, 2016.
- 5 Fountoukis, C. and Nenes, A.: ISORROPIA II: a computationally efficient thermodynamic equilibrium model for K^+ – Ca^{2+} – Mg^{2+} – NH_4^+ – Na^+ – SO_4^{2-} – NO_3^- – Cl^- – H_2O aerosols, *Atmos. Chem. Phys.*, 7, 4639–4659, doi:10.5194/acp-7-4639-2007, 2007.
- Fowler, C., Emery, W. J., Maslanik, J.: Satellite-derived evolution of Arctic sea ice age: October 1978 to March 2003. *IEEE Geosci Remote Sens Soc Lett* 1(2):71–74, doi:10.1109/LGRS.2004.824741, 2004.
- Guenther, A. B., Jiang, X., Heald, C. L., Sakulyanontvittaya, T., Duhl, T., Emmons, L. K., and Wang, X.: The Model of
10 Emissions of Gases and Aerosols from Nature version 2.1 (MEGAN2.1): an extended and updated framework for modeling biogenic emissions, *Geosci. Model Dev.*, 5, 1471–1492, doi:10.5194/gmd-5-1471-2012, 2012.
- Geldsetzer, T., Langlois, A., and Yackel, J.: Dielectric properties of brine-wetted snow on first-year sea ice, *Cold Re.g. Sci. Technol.*, 58, 47–56, doi:10.1016/j.coldregions.2009.03.009, 2009.
- Gilman, J. B., Burkhardt, J. F., Lerner, B. M., Williams, E. J., Kuster, W. C., Goldan, P. D., Murphy, P. C., Warneke, C., Fowler,
15 C., Montzka, S. A., Miller, B. R., Miller, L., Oltmans, S. J., Ryerson, T. B., Cooper, O. R., Stohl, A., and de Gouw, J. A.: Ozone variability and halogen oxidation within the Arctic and sub-Arctic springtime boundary layer, *Atmos. Chem. Phys.*, 10, 10223–10236, doi:10.5194/acp-10-10223-2010, 2010.
- Hara, K., Osada, K., Yabuki, M., and Yamanouchi, T.: Seasonal variation of fractionated sea-salt particles on the Antarctic coast, *Geophys. Res. Lett.*, 39, L18801, doi:10.1029/2012GL052761, 2012.
- 20 Hara, K., Matoba, S., Hirabayashi, M., and Yamasaki, T.: Frost flowers and sea-salt aerosols over seasonal sea-ice areas in northwestern Greenland during winter–spring, *Atmos. Chem. Phys.*, 17, 8577–8598, doi:10.5194/acp-17-8577-2017, 2017.
- Huang, J. and Jaeglé, L.: Wintertime enhancements of sea salt aerosol in polar regions consistent with a sea ice source from blowing snow, *Atmos. Chem. Phys.*, 17, 3699–3712, doi:10.5194/acp-17-3699-2017, 2017.
- Jacobi, H. W., Voisin, D., Jaffrezo, J. L., Cozic, J., and Douglas, T. A.: Chemical composition of the snowpack during the 30
25 OASIS spring campaign 2009 at Barrow, Alaska, *J. Geophys. Res.*, 117, D00R13, doi:10.1029/2011jd016654, 2012.
- Jaeglé, L., Quinn, P. K., Bates, T. S., Alexander, B., and Lin, J.-T.: Global distribution of sea salt aerosols: new constraints from in situ and remote sensing observations, *Atmos. Chem. Phys.*, 11, 3137–3157, doi:10.5194/acp-11-3137-2011, 2011.
- Jourdain, B., Preunkert, S., Cerri, O., Castebrunet, H., Udisti, R., and Legrand, M.: Year-round record of size segregated aerosol composition in central Antarctica (Concordia station): Implications for the degree of fractionation of sea-salt particles,
30 *J. Geo-phys. Res.*, 113, D14308, doi:10.1029/2007JD009584, 2008.

- Kaleschke, L., Richter, A., Burrows, J., Afe, O., Heygster, G., Notholt, J., Rankin, A. M., Roscoe, H. K., Hollwedel, J., Wagner, T., and Jacobi, H.-W.: Frost flowers on sea ice as a source of sea salt and their influence on tropospheric halogen chemistry, *Geophys. Res. Lett.*, 31, L16114, doi:10.1029/2004GL020655, 2004.
- Klimont, Z., Kupiainen, K., Heyes, C., Purohit, P., Cofala, J., Rafaj, P., Borken-Kleefeld, J., and Schöpp, W.: Global anthropogenic emissions of particulate matter including black carbon, *Atmos. Chem. Phys.*, 17, 8681–8723, doi:10.5194/acp-17-8681-2017, 2017.
- Krnavek, L., Simpson, W. R., Carlson, D., Dominé, F., Douglas, T. A., and Sturm, M.: The chemical composition of surface snow in the Arctic: examining marine, terrestrial, and atmospheric influence, *Atmos. Environ.*, 50, 349–359, doi:10.1016/j.atmosenv.2011.11.033, 2012.
- 10 Kwok, R., and D. Rothrock: Decline in Arctic sea ice thickness from submarine and ICESat records: 1958–2008, *Geophys. Res. Lett.*, 36, L15501, doi:10.1029/2009GL039035, 2009.
- [Kwok, R. and Cunningham, G.F.: Variability of Arctic sea ice thickness and volume from CryoSat-2. *Phil. Trans. R. Soc. A*, 373\(2045\), p.20140157, 2015.](#)
- Lewis, E. R. and Schwartz, S. E.: *Sea Salt Aerosol Production: Mechanisms, Methods, Measurements, and Models: A Critical*
- 15 *Review*, American Geophysical Union, Washington, D.C., 2004.
- Li, C., Hsu, N. C., Sayer, A. M., Krotkov, N. A., Fu, J. S., Lamsal, L. N., Lee, J., and Tsay, S.-C.: Satellite observation of pollutant emissions from gas flaring activities near the Arctic, *Atmos. Environ.*, 133, 1–11, doi:10.1016/j.atmosenv.2016.03.019, 2016.
- Li, M., Zhang, Q., Kurokawa, J.-I., Woo, J.-H., He, K., Lu, Z., Ohara, T., Song, Y., Streets, D. G., Carmichael, G. R., Cheng,
- 20 Y., Hong, C., Huo, H., Jiang, X., Kang, S., Liu, F., Su, H., and Zheng, B.: MIX: a mosaic Asian anthropogenic emission inventory under the international collaboration framework of the MICS-Asia and HTAP, *Atmos. Chem. Phys.*, 17, 935-963, doi:10.5194/acp-17-935-2017, 2017.
- Lin, J.-T. and McElroy, M. B.: Detection from space of a reduction in anthropogenic emissions of nitrogen oxides during the Chinese economic downturn, *Atmos. Chem. Phys.*, 11, 8171-8188, doi:10.5194/acp-11-8171-2011, 2011.
- 25 Lin, S.-J. and Rood, R. B.: Multidimensional flux-form semi-Lagrangian transport schemes, *Mon. Weather Rev.*, 124, 2046–2070, doi:10.1175/1520-0493(1996)124<2046:MFFSLT>2.0.CO;2, 1996.
- Liu, H., Jacob, D. J., Bey, I., and Yantosca, R. M.: Constraints from ²¹⁰Pb and ⁷Be on wet deposition and transport in a global three-dimensional chemical tracer model driven by assimilated meteorological fields, *J. Geophys. Res.*, 106(D11), 12 109–12 128, doi:10.1029/2000JD900839, 2001.

Liu, Z. Y., Vaughan, M., Winker, D., Kittaka, C., Getzewich, B., Kuehn, R., Omar, A., Powell, K., Trepte, C., and Hostetler, C.: The CALIPSO Lidar Cloud and Aerosol Discrimination: Version 2 Algorithm and Initial Assessment of Performance, *J. Atmos. Ocean. Tech.*, 26, 1198–1213, doi:10.1175/2009JTECHA1229.1, 2009.

5 [Mann, G. W., Anderson, P. S., and Mobbs, S. D.: Profile measurements of blowing snow at Halley, Antarctica, *J. Geophys. Res.*, 105, 24,491–24,508, 2000.](#)

Mao, J., Jacob, D. J., Evans, M. J., Olson, J. R., Ren, X., Brune, W. H., Clair, J. M. St., Crouse, J. D., Spencer, K. M., Beaver, M. R., Wennberg, P. O., Cubison, M. J., Jimenez, J. L., Fried, A., Weibring, P., Walega, J. G., Hall, S. R., Weinheimer, A. J., Cohen, R. C., Chen, G., Crawford, J. H., McNaughton, C., Clarke, A. D., Jaeglé, L., Fisher, J. A., Yantosca, R. M., Le Sager, P., and Carouge, C.: Chemistry of hydrogen oxide radicals (HOx) in the Arctic troposphere in spring, *Atmos. Chem. Phys.*, 10, 5823–5838, doi:10.5194/acp-10-5823-2010, 2010.

Mao, J., Fan, S., Jacob, D. J., and Travis, K. R.: Radical loss in the atmosphere from Cu-Fe redox coupling in aerosols, *Atmos. Chem. Phys.*, 13, 509–519, doi:10.5194/acp-13-509-2013, 2013.

Martin, S.: A field study of brine drainage and oil entrapment in first-year sea ice., *J. of Glaciol*, 22 (88), 473–502, 1979.

Maslanik, J. A., Fowler, C., Stroeve, J., Drobot, S., Zwally, H. J., Yi, D., Emery, W.J.: A younger, thinner ice cover: increased potential for rapid, extensive ice loss. *Geophys. Res. Lett.* 34: L24501. doi:10.1029/2007GL032043, 2007.

15 [Massom, R. A., Eicken, H., Hass, C., Jeffries, M. O., Drinkwater, M. R., Sturm, M., Worby, A. P., Wu, X., Lytle, V. I., Ushio, S., Morris, K., Reid, P. A., Warren, S. G., and Allison, I.: Snow on Antarctic sea ice, *Rev. Geophys.*, 39, 413–445, doi:10.1029/2000RG000085, 2001.](#)

20 [May, N. W., Quinn, P. K., McNamara, S. M., and Pratt, K. A.: Multiyear study of the dependence of sea salt aerosol on wind speed and sea ice conditions in the coastal Arctic, *J. Geophys. Res. Atmos.*, 121, 9208–9219, doi:10.1002/2016JD025273, 2016.](#)

Mundy, C.J., Barber, D.G. and Michel, C.: Variability of snow and ice thermal, physical and optical properties pertinent to sea ice algae biomass during spring, *J. Mar. Syst.*, 58, 107–120, doi:10.1016/j.jmarsys.2005.07.003, 2005.

25 Nandan, V., Geldsetzer, T., Yackel, J., Mahmud, M., Scharien, R., Howell, S., King, J., Ricker, R. and Else, B.: Effect of Snow Salinity on CryoSat-2 Arctic First-Year Sea Ice Freeboard Measurements, *Geophys. Res. Lett.*, 44(20), doi:10.1002/2017GL074506, 2017.

Nakawo, M. and Sinha, N.K.: Growth rate and salinity profile of first-year sea ice in the high Arctic. *J. Glaciol*, 27(96), pp.315–330, doi: DOI: 10.1017/ S0022143000015409, 1981.

30 [Nilsson, E. D., Rannik, U., Swietlicki, E., Leck, C., Aalto, P. P., Zhou, J., and Norman, M.: Turbulent aerosol fluxes over the Arctic Ocean 2, Wind-driven sources from the sea, *J. Geophys. Res.*, 106, 32111–32124, 2001.](#)

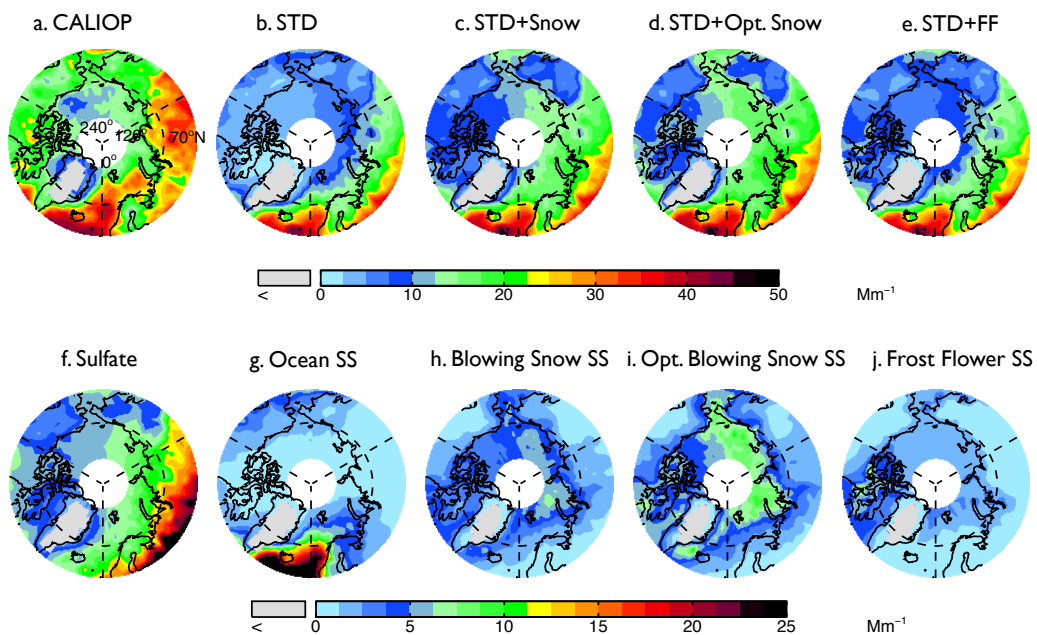
- Rankin, A. M., Auld, V., and Wolff, E. W.: Frost flowers as a source of fractionated sea salt aerosol in the polar regions, *Geophys. Res. Lett.*, 27, 3469–3472, doi:10.1029/2000GL011771, 2000.
- Renner, A.H., Gerland, S., Haas, C., Spreen, G., Beckers, J.F., Hansen, E., Nicolaus, M. and Goodwin, H.: Evidence of Arctic sea ice thinning from direct observations. *Geo. Res. Lett.*, 41(14), pp.5029-5036, doi:10.1002/2014GL060369, 2014.
- 5 Reynolds, R. W., Rayner, N. A., Smith, T. M., Stokes, D. C., and Wang, W.: An improved in situ and satellite SST analysis for climate, *J. Clim.*, 15, 1609–1625, doi:10.1175/1520-0442(2002)015<1609:AIISAS>2.0.CO;2, 2002.
- Rienecker, M. M., Suarez, M. J., Gelaro, R., Todling, R., Bacmeister, J., Liu, E., Bosilovich, M. G., Schubert, S. D., Takacs, L., Kim, G.-K., Bloom, S., Junye, C., Collins, D., Conaty, A., da Silva, A., Gu, W., Joiner, J., Koster, R. D., Lucchesi, R., Molod, A., Owens, T., Pawson, S., Pegion, P., Redder, C. R., Reichle, R., Robertson, F. R., Ruddick, A. G., Sienkiewicz, M.,
10 and Woollen, J.: MERRA: NASA’s modern-era retrospective analysis for research and applications, *J. Climate*, 24, 3624–3648, doi:10.1175/JCLI-D-11-00015.1, 2011.
- Roscoe, H. K., Brooks, B., Jackson, A. V., Smith, M. H., Walker, S. J., Obbard, R. W., and Wolff, E. W.: Frost flowers in the laboratory: Growth, characteristics, aerosol, and the underlying sea ice, *J. Geophys. Res.*, 116, D12301, doi:10.1029/2010JD015144, 2011.
- 15 Schroeder, W. H., Anlauf, K. G., Barrie, L. A., Lu, J. Y., Steffen, A., Schneeberger, D. R., and Berg, T.: Arctic springtime depletion of mercury, *Nature*, 394, 331–332, doi:10.1038/28530, 1998.
- Seguin, A.M., Norman, A.L. and Barrie, L.: Evidence of sea ice source in aerosol sulfate loading and size distribution in the Canadian High Arctic from isotopic analysis, *J. Geophys. Res. Atmos.*, 119, 1087–1096, doi:10.1002/2013JD020461, 2014.
- Seibert, P. and Frank, A.: Source-receptor matrix calculation with a Lagrangian particle dispersion model in backward mode,
20 *Atmos. Chem. Phys.*, 4, 51-63, doi:10.5194/acp-4-51-2004, 2004.
- Shaw, P. M., Russell, L. M., Jefferson, A., and Quinn, P. K.: Arctic organic aerosol measurements show particles from mixed combustion in spring haze and from frost flowers in winter, *Geophys. Res. Lett.*, 37, L10803, doi:10.1029/2010GL042831, 2010.
- Simpson, W. R., Carlson, D., Hönninger, G., Douglas, T. A., Sturm, M., Perovich, D., and Platt, U.: First-year sea-ice contact
25 predicts bromine monoxide (BrO) levels at Barrow, Alaska better than potential frost flower contact, *Atmos. Chem. Phys.*, 7, 621-627, doi:10.5194/acp-7-621-2007, 2007.
- Slinn, S.A. and Slinn, W.G.N.: Predictions for particle deposition on natural waters. *Atmospheric Environment* (1967), 14(9), pp.1013-1016, doi:10.1016/0004-6981(80)90032-3, 1980.
- Stammerjohn, S., Massom, R., Rind, D. and Martinson, D.: Regions of rapid sea ice change: An inter-hemispheric seasonal
30 comparison. *Geo. Res. Lett.*, 39(6), doi:10.1029/2012GL050874, 2012.

- Steffen, A., Douglas, T., Amyot, M., Ariya, P., Aspö, K., Berg, T., Bottenheim, J., Brooks, S., Cobbett, F., Dastoor, A., Dommergue, A., Ebinghaus, R., Ferrari, C., Gardfeldt, K., Goodsite, M. E., Lean, D., Poulain, A. J., Scherz, C., Skov, H., Sommar, J., and Temme, C.: A synthesis of atmospheric mercury depletion event chemistry in the atmosphere and snow, *Atmos. Chem. Phys.*, 8, 1445-1482, doi:10.5194/acp-8-1445-2008, 2008.
- 5 Stohl, A., Hittenberger, M., and Wotawa, G.: Validation of the Lagrangian particle dispersion model FLEXPART against large scale tracer experiment data, *Atmos. Environ.*, 32, 4245–4264, doi:10.1016/S1352-2310(98)00184-8, 1998.
- Stohl, A., Forster, C., Frank, A., Seibert, P., and Wotawa, G.: Technical note: The Lagrangian particle dispersion model FLEXPART version 6.2, *Atmos. Chem. Phys.*, 5, 2461-2474, doi:10.5194/acp-5-2461-2005, 2005.
- Travis, K. R., Jacob, D. J., Fisher, J. A., Kim, P. S., Marais, E. A., Zhu, L., Yu, K., Miller, C. C., Yantosca, R. M., Sulprizio, M. P., Thompson, A. M., Wennberg, P. O., Crouse, J. D., St. Clair, J. M., Cohen, R. C., Laughner, J. L., Dibb, J. E., Hall, S. R., Ullmann, K., Wolfe, G. M., Pollack, I. B., Peischl, J., Neuman, J. A., and Zhou, X.: Why do models overestimate surface ozone in the Southeast United States?, *Atmos. Chem. Phys.*, 16, 13561– 13577, doi:10.5194/acp-16-13561-2016, 2016.
- 10 Turner, J., Comiso, J.C., Marshall, G.J., Lachlan-Cope, T.A., Bracegirdle, T., Maksym, T., Meredith, M.P., Wang, Z. and Orr, A.: Non-annular atmospheric circulation change induced by stratospheric ozone depletion and its role in the recent increase of Antarctic sea ice extent. *Geo., Res. Lett.*, 36(8), doi:10.1029/2009GL037524, 2009.
- 15 Obbard, R. W., Roscoe, H.K., Wolff, E. W., and Atkinson, H. M.: Frost flower surface area and chemistry as a function of salinity and temperature, *J. Geophys. Res.*, 114, D20305, doi:10.1029/2009JD012481, 2009.
- Olivier, J. G. J. and Berdowski, J. J. M.: Global emissions sources and sinks, in: *The Climate System*, Berdowski, J., Guicherit, R. and B. J. Heij (eds.), A.A. Balkema Publishers/Swets & Zeitlinger Publishers, Lisse, The Netherlands, ISBN 90 5809 255 0, 33-78, 2001.
- 20 Palm, S. P., Yang, Y. K., Spinhirne, J. D., and Marshak, A.: Satellite remote sensing of blowing snow properties over Antarctica, *J. Geophys. Res.-Atmos.*, 116, 1–16, doi:10.1029/2011jd015828, 2011.
- Palm, S. P., Kayetha, V., Yang, Y., and Pauly, R.: Blowing snow sublimation and transport over Antarctica from 11 years of CALIPSO observations, *The Cryosphere*, 11, 2555-2569, doi:10.5194/tc-11-2555-2017, 2017.
- 25 Parkinson, C. L. and Cavalieri, D. J.: Antarctic sea ice variability and trends, 1979–2010, *The Cryosphere*, 6, 871-880, doi:10.5194/tc-6-871-2012, 2012.
- Perovich, D. K. and Richter-Menge, J. A.: Surface characteristics of lead ice, *J. Geophys. Res.*, 99, 16341–16350, doi:10.1029/94JC01194, 1994.

- Pye, H. O. T., Liao, H., Wu, S., Mickley, L. J., Jacob, D. J., Henze, D. K., and Seinfeld, J. H.: Effect of changes in climate and emissions on future sulfate-nitrate-ammonium aerosol levels in the United States, *J. Geophys. Res.*, 114, D01205, doi:10.1029/2008JD010701, 2009.
- Udisti, R., Dayan, U., Becagli, S., Busetto, M., Frosini, D., Legrand, M., Lucarelli, F., Preunkert, S., Severi, M., Traversi, R., and Vitale, V.: Sea spray aerosol in central Antarctica. Present atmospheric behaviour and implications for paleoclimatic reconstructions, *Atmos. Environ.*, 52, 109–120, doi:10.1016/j.atmosenv.2011.10.018, 2012.
- van der Werf, G. R., Randerson, J. T., Giglio, L., Collatz, G. J., Mu, M., Kasibhatla, P. S., Morton, D. C., DeFries, R. S., Jin, Y., and van Leeuwen, T. T.: Global fire emissions and the contribution of deforestation, savanna, forest, agricultural, and peat fires (1997–2009), *Atmos. Chem. Phys.*, 10, 11707–11735, doi:10.5194/acp-10-11707-2010, 2010.
- van Donkelaar, A., Martin, R. V., Leaitch, W. R., Macdonald, A. M., Walker, T. W., Streets, D. G., Zhang, Q., Dunlea, E. J., Jimenez, J. L., Dibb, J. E., Huey, L. G., Weber, R., and Andreae, M. O.: Analysis of aircraft and satellite measurements from the Intercontinental Chemical Transport Experiment (INTEX-B) to quantify long-range transport of East Asian sulfur to Canada, *Atmos. Chem. Phys.*, 8, 2999–3014, doi:10.5194/acp-8-2999-2008, 2008.
- Wagenbach, D., Ducroz, F., Mulvaney, R., Keck, L., Minikin, A., Legrand, M., Hall, J. S., and Wolff, E. W.: Sea-salt aerosol in coastal Antarctic regions, *J. Geophys. Res.*, 103, 961–974, doi:10.1029/97JD01804, 1998.
- Wang, Y., D.J. Jacob, and J.A. Logan, Global simulation of tropospheric O₃-NO_x-hydrocarbon chemistry, 1. Model formulation, *J. Geophys. Res.*, 103, D9,10,713–10,726, doi:10.1029/98JD00158, 1998.
- Wang, Q., Jacob, D. J., Fisher, J. A., Mao, J., Leibensperger, E. M., Carouge, C. C., Le Sager, P., Kondo, Y., Jimenez, J. L., Cubison, M. J., and Doherty, S. J.: Sources of carbonaceous aerosols and deposited black carbon in the Arctic in winter-spring: implications for radiative forcing, *Atmos. Chem. Phys.*, 11, 12453–12473, doi:10.5194/acp-11-12453-2011, 2011.
- [Warren, S. G., Rigor, I. G., Untersteiner, N., Radionov, V. F., Bryazgin, N. N., Aleksandrov, Ye. I., and Colony, R.: Snow depth on Arctic sea ice, *J. Climate*, 12, 1814–1829, 1999.](#)
- Weeks, W. F., and Lee O. S.: Observations on the physical properties of sea-ice at Hopedale, Labrador, Arctic, 11(3), 135–155, doi: 10.14430/arctic3740, 1958.
- Weeks, W. F. and Ackley, S. F.: The growth, structure and properties of sea ice, 9–164, Plenum Press, New York, 1986.
- Weller, R., Woltjen, J., Piel, C., Resenberg, R., Wagenbach, D., König-Langlo, G., and Kriews, M.: Seasonal variability of crustal and marine trace elements in the aerosol at Neumayer station, Antarctica, *Tellus*, 60, 742–752, doi:10.1111/j.1600-0889.2008.00372.x, 2008.
- Wesely, M. L., Parameterization of surface resistance to gaseous dry deposition in regional-scale numerical models, *Atmos. Environ.*, 23, 1293–1304, doi:10.1016/0004-6981(89)90153-4, 1989.

- Winker, D. M., Vaughan, M. A., Omar, A., Hu, Y., and Powell, J. A.: Overview of the CALIPSO Mission and CALIOP Data Processing Algorithms, *J. Atmos. Ocean. Tech.*, 26, 2310–2323, doi:10.1175/2009JTECHA1281.1, 2009.
- Winker, D. M., Tackett, J. L., Getzewich, B. J., Liu, Z., Vaughan, M. A., and Rogers, R. R.: The global 3-D distribution of tropospheric aerosols as characterized by CALIOP, *Atmos. Chem. Phys.*, 13, 3345-3361, doi:10.5194/acp-13-3345-2013, 5 2013.
- Winker, D.: CALIPSO LID L2 Standard HDF File -Version 4.10. NASA Langley Research Center Atmospheric Science Data Center DAAC. https://doi.org/10.5067/CALIOP/CALIPSO/LID_L2_05kmAPro-Standard-V4-10, Last Access February 2018, 2016
- Wolff, E. W., Fischer, H., Fundel, F., Ruth, U., Twarloh, B., Littot, G. C., Mulvaney, R., Rothlisberger, R., de Angelis, M., 10
Boutron, C. F., Hansson, M., Jonsell, U., Hutterli, M. A., Bigler, M., Lambeck, K., Kaufmann, P., Stauffer, B., Stocker, T. F., Steffensen, J. P., Siggaard-Andersen, M. L., Udisti, R., Becagli, S., Castellano, E., Severi, M., Wagenbach, D., Barbante, C., Gabrielli, P., and Gaspari, V.: Southern Ocean sea-ice extent, productivity and iron flux over the past eight glacial cycles, *Nature*, 440, 491–496, doi:10.1038/nature04614, 2006.
- 15 [Worby, A.P., Massom, R.A., Allison, I., Lytle, V.I. and Heil, P.: East Antarctic sea ice: A review of its structure, properties and drift. *Antarctic sea ice: physical processes, interactions and variability*, pp.41-67, 1998.](#)
- Xu, L., Russell, L. M., Somerville, R. C. J., and Quinn, P. K.: Frost flower aerosol effects on Arctic wintertime longwave cloud radiative forcing, *J. Geophys. Res.-Atmos.*, 118, 13282–13291, doi:10.1002/2013JD020554, 2013.
- Xu, J.-W., Martin, R. V., Morrow, A., Sharma, S., Huang, L., Leaitch, W. R., Burkart, J., Schulz, H., Zanatta, M., Willis, M. D., Henze, D. K., Lee, C. J., Herber, A. B., and Abbatt, J. P. D.: Source attribution of Arctic black carbon constrained by 20
aircraft and surface measurements, *Atmos. Chem. Phys.*, 17, 11971-11989, doi:10.5194/acp-17-11971-2017, 2017.
- Yang, X., Pyle, J. A., and Cox, R. A.: Sea salt aerosol production and bromine release: Role of snow on sea ice, *Geophys. Res. Lett.*, 35, L16815, doi:10.1029/2008GL034536, 2008.
- Yang, X., Pyle, J. A., Cox, R. A., Theys, N., and Van Roozendaal, M.: Snow-sourced bromine and its implications for polar tropospheric ozone, *Atmos. Chem. Phys.*, 10, 7763-7773, doi:10.5194/acp-10-7763-2010, 2010.
- 25 Yang, X., Neděla, V., Runštuk, J., Ondrušková, G., Krausko, J., Vetráková, Ľ., and Heger, D.: Evaporating brine from frost flowers with electron microscopy and implications for atmospheric chemistry and sea-salt aerosol formation, *Atmos. Chem. Phys.*, 17, 6291-6303, doi:10.5194/acp-17-6291-2017, 2017.
- Zender, C. S.: Mineral Dust Entrainment and Deposition (DEAD) model: Description and 1990s dust climatology, *J. Geophys. Res.*, 108, doi:10.1029/2002JD002775, 2003.

Zhang, L., Gong, S., Padro, J., and Barrie, L.: A size-segregated particle dry deposition scheme for an atmospheric aerosol module, *Atmos. Environ.*, 35, 549–560, doi: /10.1016/S1352-2310(00)00326-5, 2001.



5 **Figure 1: Spatial distribution of mean aerosol extinction coefficients (0-2 km) during the 2007-2009 Arctic cold season (November-**
April) observed by (a) CALIOP and calculated with the GEOS-Chem model in (b) a Standard simulation (STD), (c) a simulation
including blowing snow SSA emissions (STD+Snow), (d) an optimized blowing snow simulation (STD+Opt. Snow), and (e)
a simulation including frost flower SSA emissions (STD+FF). The simulated extinctions are sampled at the time and location of the
CALIOP overpasses, and the CALIOP sensitivity threshold is applied. The bottom panels show the extinction coefficients of
 10 **individual aerosol components in the GEOS-Chem simulations: (f) sulfate aerosol, (g) open ocean SSA, (h) blowing snow SSA, (i)**
Opt. blowing snow SSA and (j) frost flower SSA. Note the different colorbar scales for the top and bottom rows.

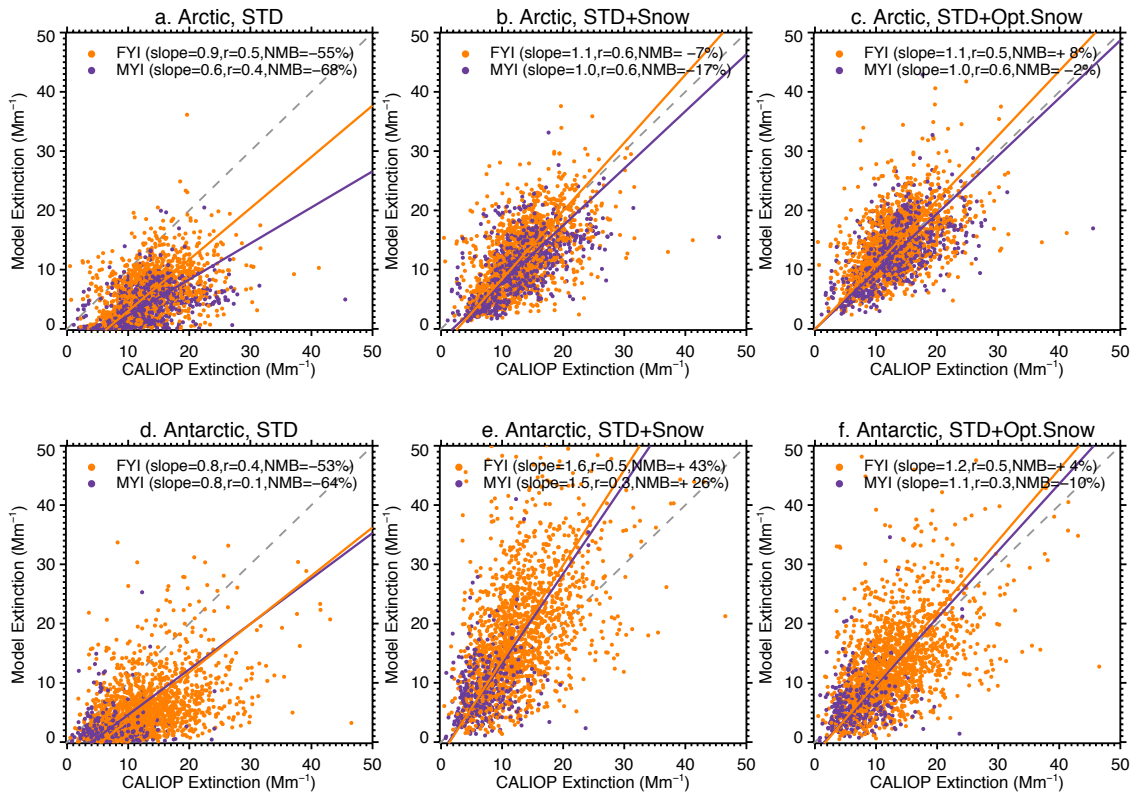


Figure 2. Scatter plot of CALIOP and GEOS-Chem aerosol extinction coefficients over FYI (orange circles) and MYI (purple circles) for the Arctic cold season (November–April, top panels) and Antarctic cold season (May–October, bottom panels). Each symbol represents the monthly aerosol extinction coefficients for individual grid boxes (2°x5°, 0–2 km) over sea ice. The dashed gray line is the 1:1 line. The purple and orange lines are the linear fit for the points over MYI and FYI, respectively. The slope of the regression line, correlation coefficient (r) and normalized mean bias, $NMB = 100 \times (\text{Model}/\text{Obs} - 1)$, are given in the insert of each figure.

5

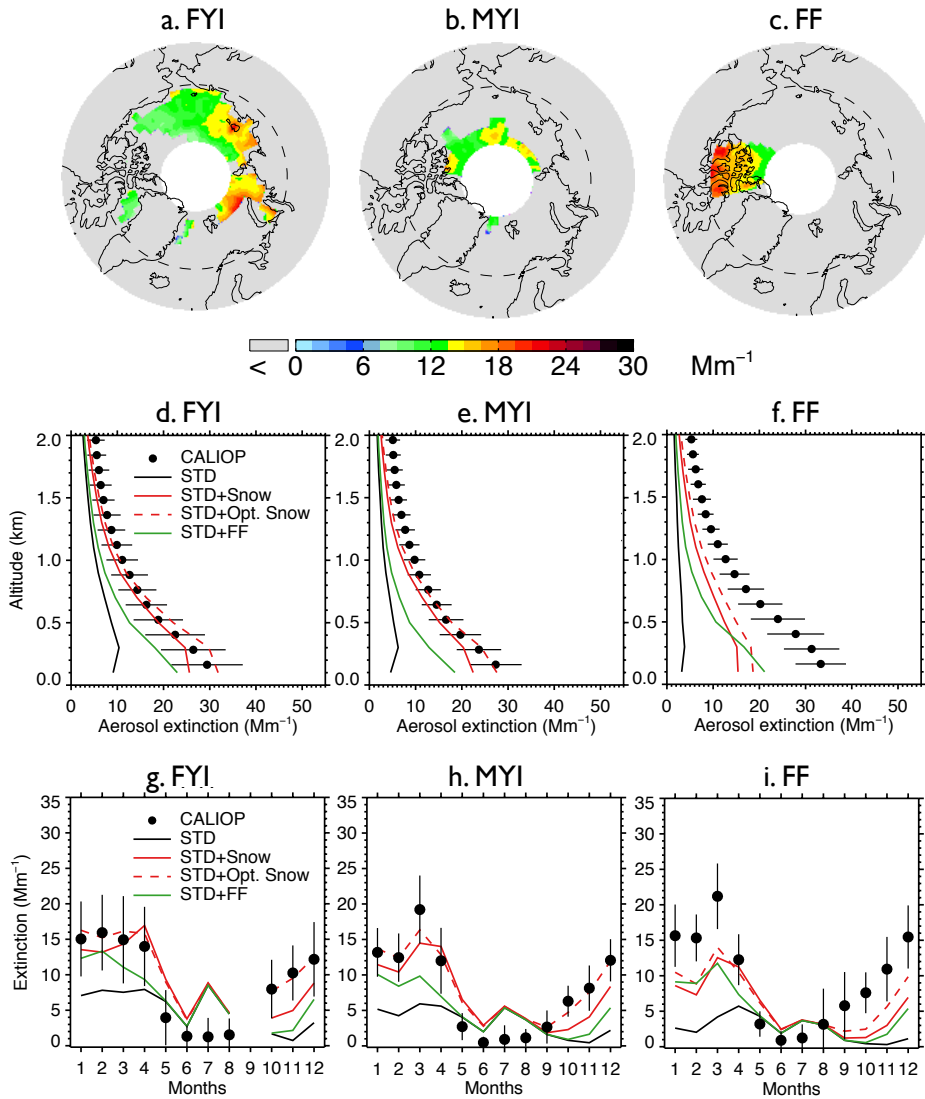


Figure 3: Top row: 2007–2009 CALIOP mean aerosol extinction coefficients (0–2 km) in the Arctic cold season (November–April) over (a) first-year sea ice (FYI), (b) multi-year sea ice (MYI) and (c) the Canadian Arctic Archipelago (CAA). Middle row: Vertical profiles of Arctic cold season mean aerosol extinction coefficients over (d) FYI, (e) MYI and (f) CAA for CALIOP (black dots with horizontal lines indicating standard deviations) and GEOS-Chem model simulations (STD: black lines, STD+Snow: red solid lines, STD+Opt. Snow: red dashed lines; STD+FF: green lines). Bottom row: Seasonal cycle of 0–2 km monthly aerosol extinction coefficients averaged over (g) FYI, (h) MYI and (i) CAA. CALIOP observations are shown as black circles and vertical lines indicate the interannual standard deviation. The four GEOS-Chem model simulations are also shown (STD: black lines, STD+Snow: red solid lines, STD+Opt. Snow: red dashed lines, STD+FF: green lines).

5

10

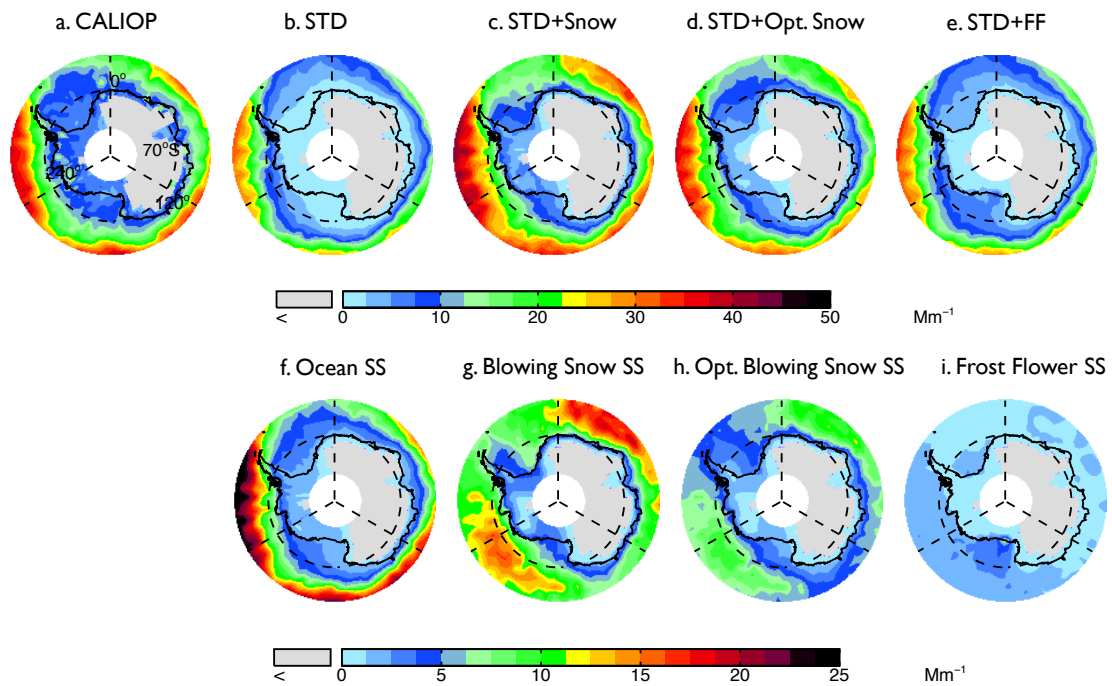


Figure 4. Spatial distributions of mean aerosol extinction coefficients (0–2 km) during the 2007–2009 Antarctic cold season (May–October) observed by (a) CALIOP and calculated with the GEOS-Chem (b. STD, c. STD+Snow, d. STD+Opt. Snow–2, e. STD+FF). The bottom panels show extinctions of individual aerosol components in the GEOS-Chem simulations: (f) open ocean SSA, (g) blowing snow SSA, (h) Opt. blowing snow SSA and (i) frost flower SSA. Note the different colorbar scales for the top and bottom rows.

5

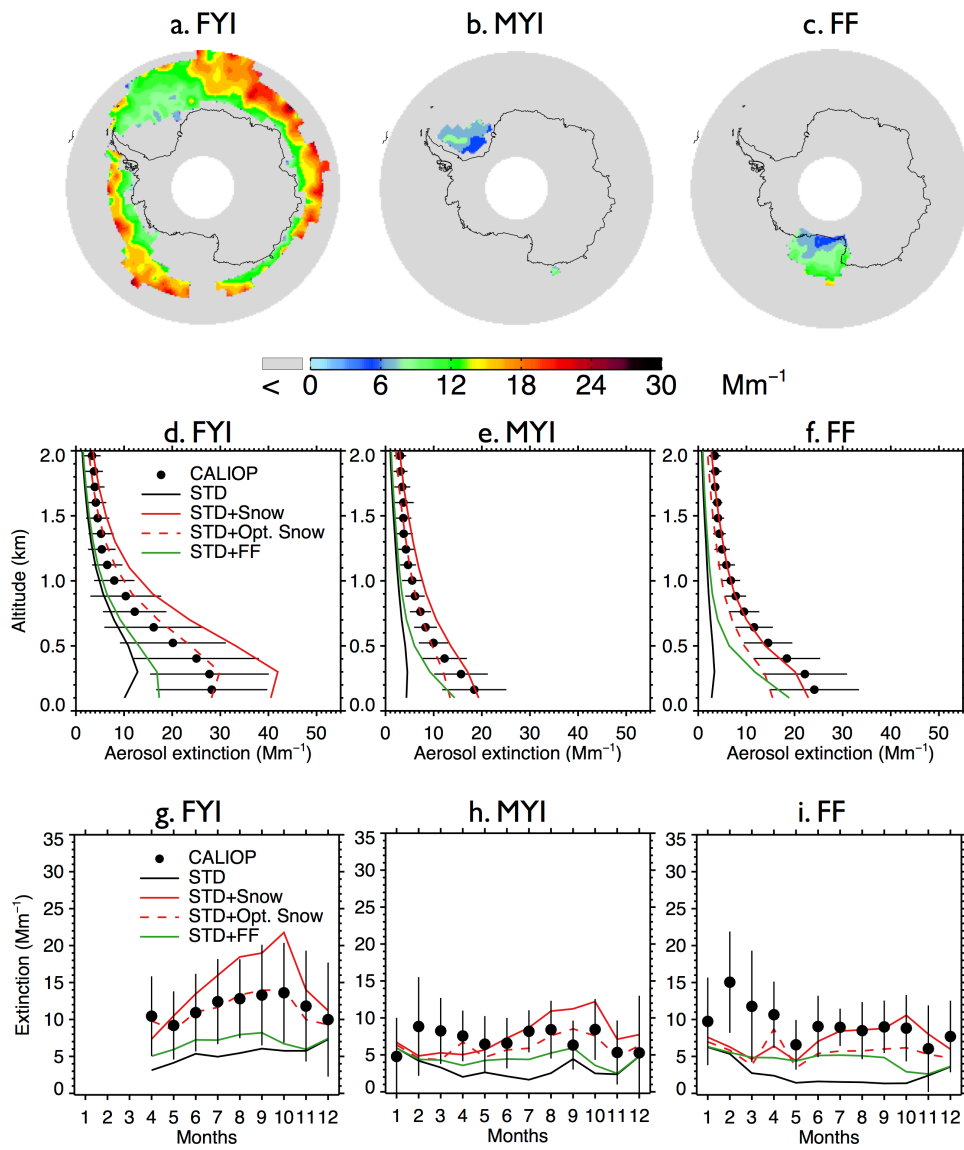


Figure 5. Same as Figure 3, but for Antarctic aerosol extinction coefficients during Austral winter (May–October) over (a) FYI (excluding offshore Ross Ice-shelf), (b) MYI and (c) offshore Ross Ice-shelf. As shown in (g), the monthly average aerosol extinction coefficients are not available over FYI during Antarctic summer (January–March) due to the limited FYI extent.

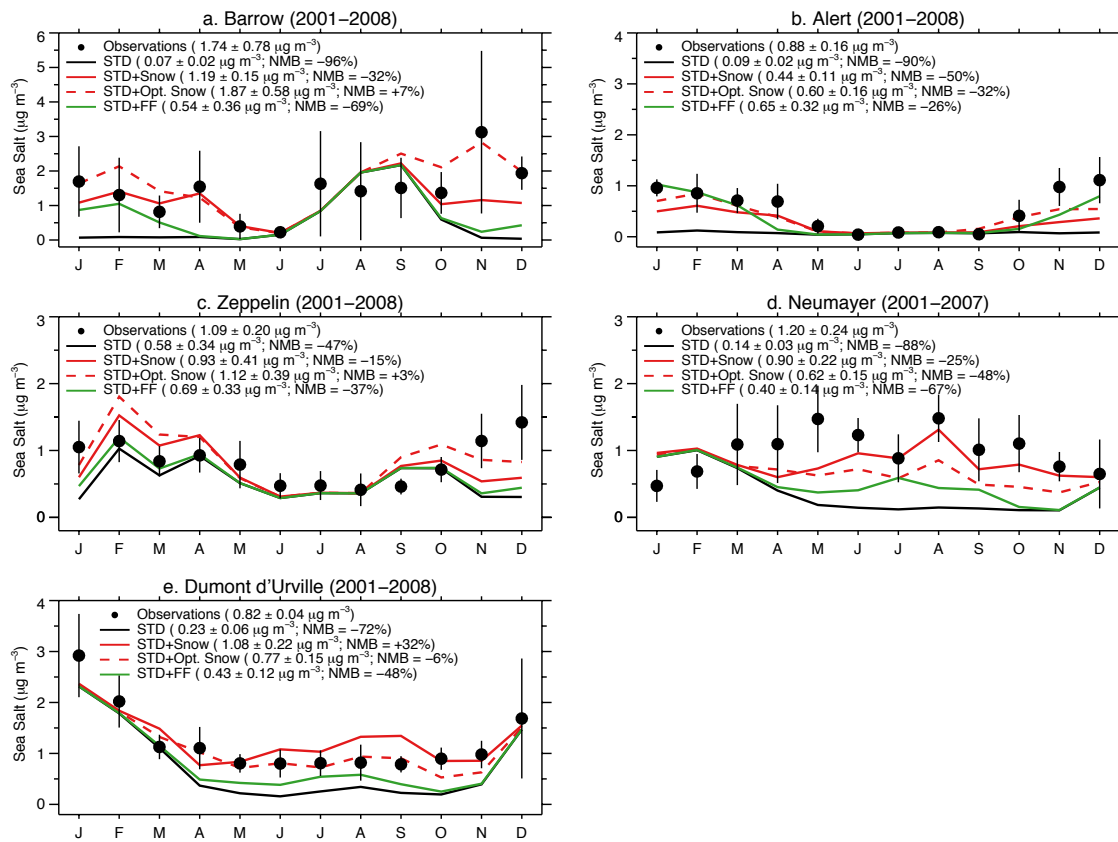


Figure 6. Monthly mean SSA mass concentrations at Arctic sites (a. Barrow, b. Alert, c. Zeppelin) and Antarctic sites (d. Dumont d'Urville, e. Neumayer). All observations and model results are for 2001–2008 except at Neumayer (2001–2007). The observed mean concentrations are indicated with filled black circles, and the lines are for the GEOS-Chem simulations (STD: black line, STD+Snow: red line, STD+Opt. Snow: red dashed line; STD+FF: green line). The black vertical lines are the standard deviations of monthly means for the observation years. For each individual panel, the insert lists mean concentrations and standard deviations, as well as the NMB for the cold season only (Arctic: November–April; Antarctic: May–October).

5

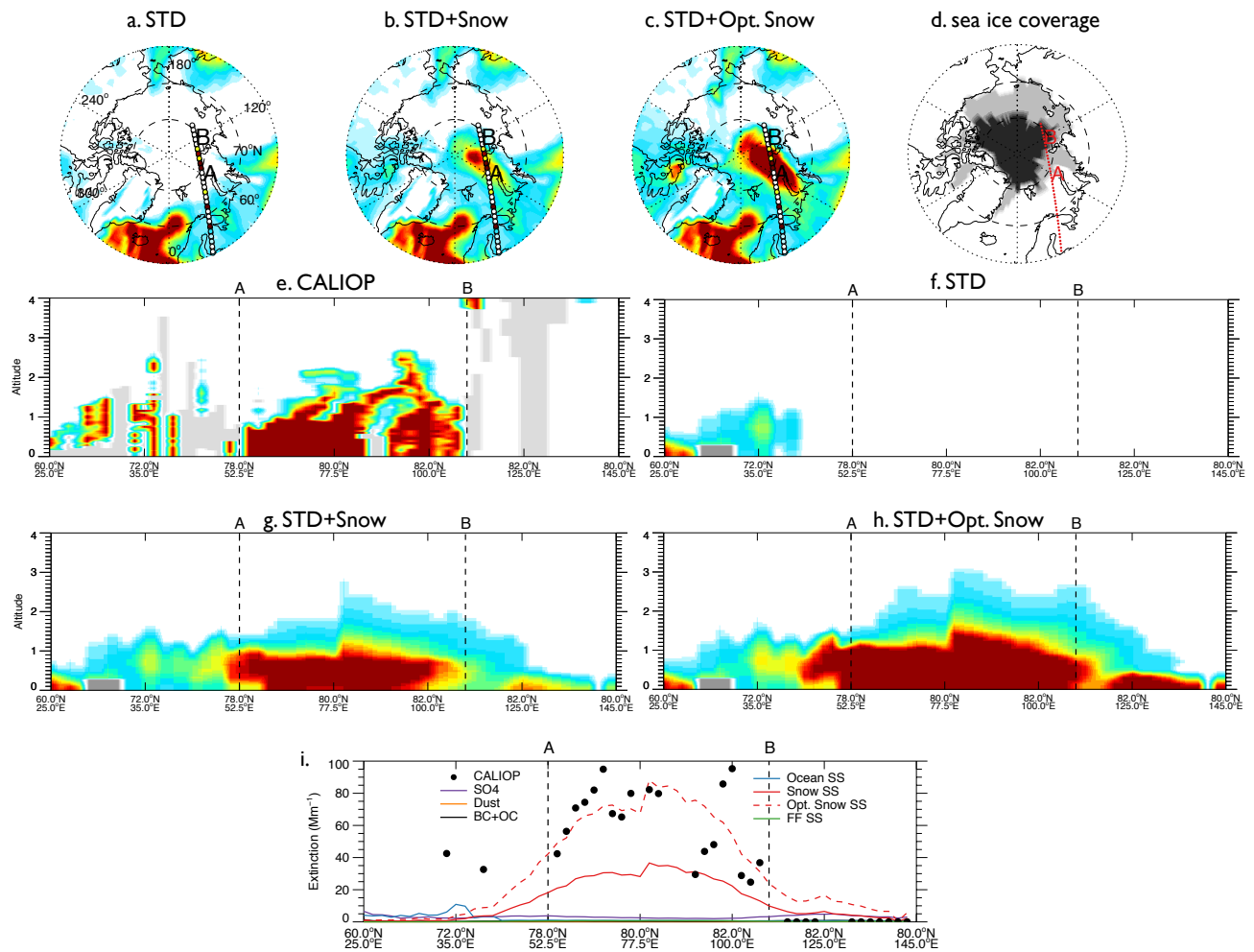
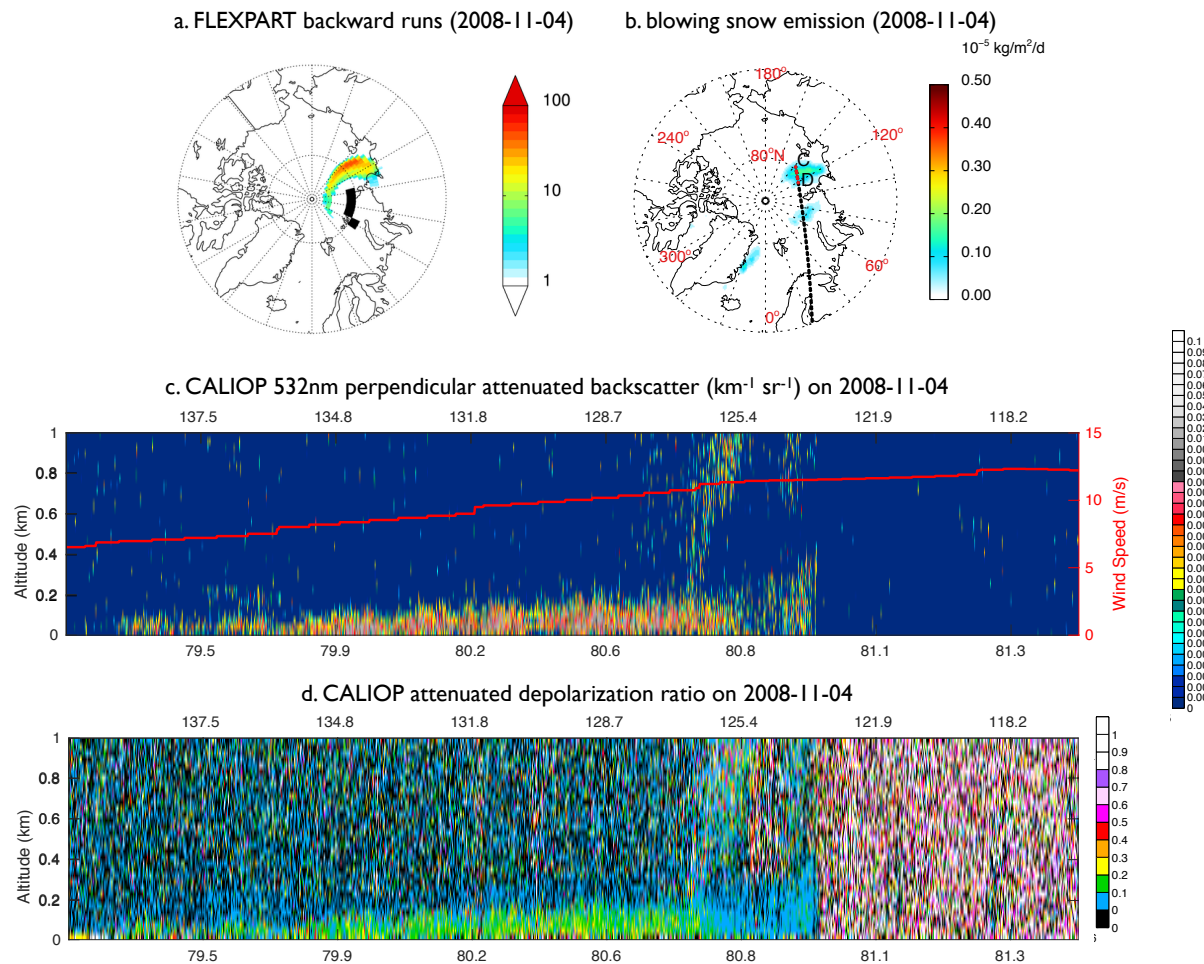


Figure 7. November 6, 2008 case study of a blowing snow SSA feature over the Arctic. Top panels: Spatial distribution of mean aerosol extinctions below 2 km altitude for the (a) STD, (b) STD+Snow, and (c) STD+Opt. Snow GEOS-Chem simulations. The CALIOP nighttime overpass at 00:58–01:12 UTC is displayed on the top panels, with filled circles color-coded according to observed mean extinction coefficients below 2 km. The overpass intercepts the SSA blowing snow feature between points A and B. Panel (d) shows the MERRA sea ice coverage on November 6, 2008, with light gray shading indicating FYI and black shading for MYI. Panels (e–h) show the observed and simulated vertical cross-sections of aerosol extinction coefficients along the CALIOP overpass. The light gray shading in (e) indicates that no valid data is available for CALIOP. The dark gray shading in (f–h) shows the local topography in the model. Panel (i) shows the 0–2 km CALIOP mean aerosol extinctions and the contributions of different aerosol types in the GEOS-Chem simulations.



5 **Figure 8.** (a) The November 4, 2008 FLEXPART footprint below 100m (in seconds) for particles initialized at 0-2 km over the black squares on November 6, 2008, near the blowing snow feature observed by CALIOP (Figure 7). (b) November 4, 2008 blowing snow SSA emissions from the STD+Snow simulation, and the CALIOP overpass at 01:11–01:24 UTC on that day. The bottom two panels display CALIOP cross-sections between points C and D for (c) the 532nm perpendicular attenuated backscatter ($\text{km}^{-1} \text{ sr}^{-1}$) and (d) attenuated depolarization ratio. The surface wind speeds (m s^{-1}) are shown with a red line in panel c.

Supplement for “Using CALIOP to constrain blowing snow emissions of sea salt aerosols over Arctic and Antarctic sea ice”

1 Combining daytime and nighttime CALIOP observations to calculate nighttime-equivalent extinction coefficients

The daytime CALIOP estimates of aerosol extinction coefficients have higher sensitivity threshold than the nighttime estimates due to the noise from solar photons (Winker et al., 2009), making nighttime extinctions more accurate. Over polar regions during summer, however, nighttime CALIOP observations are very limited due to constant solar illumination. In order to examine the seasonal variation in CALIOP aerosol extinction coefficients over polar regions, we calculate nighttime-equivalent CALIOP aerosol extinction coefficients following the approach of Di Pierro et al. (2013). The nighttime-equivalent aerosol extinction is the weighted average of nighttime and adjusted daytime aerosol extinctions. The daytime aerosol extinctions are adjusted with a scaling factor, which takes into account the different sampling frequency of daytime and nighttime observations. The nighttime-equivalent aerosol extinction coefficient (ϵ_{neq}) is calculated following Eq. (1):

$$\epsilon_{\text{neq}} = (f_n \cdot \epsilon_n \cdot N_n + f_d \cdot \text{SF} \cdot \epsilon_d' \cdot N_d) / (N_n + N_d), \quad (1)$$

where f is the aerosol detection frequency and the subscripts of d and n correspond to the daytime and nighttime. The ϵ symbol denotes the observed aerosol extinction coefficient, and $\epsilon_d' = \epsilon_d / 1.6$, which is scaled to take into the account of higher sensitivity threshold of daytime data (See following and Fig. S1a). SF is a scaling factor taking into account the different detection sensitivities of daytime and nighttime retrievals. N is the number of CALIOP samplings.

In the absence of daytime data, we have

$$\epsilon_{\text{neq}} = f_n \cdot \epsilon_n \quad (2)$$

as we assign undetected aerosol layers (or clear air) an extinction coefficient value of 0.0 km^{-1} .

20

The scaling factor, SF, is defined as $\text{SF} = f_n / f_d$ based on the relationship between SF and backscatter coefficient during winter months (November-April for the Arctic and May-October for the Antarctic) over the $62\text{-}70^\circ \text{ N/S}$ latitude band following Di Pierro et al. (2013).

Figure S1c shows that both daytime and nighttime aerosol detection frequency decrease with height during Arctic ($62\text{-}70^\circ \text{ N}$) winter (October-April 2007-2009), with the daytime detection frequency being 1.5-8 times lower than the nighttime detection frequency. The average daytime aerosol backscatter coefficients are $\sim 60\%$ higher than the nighttime ones, as the daytime

25

profiles have a higher sensitivity threshold and do not detect faint aerosol layers with lower aerosol extinctions. Scaling the daytime aerosol backscatter coefficients by 0.6 ($\beta'_d = \beta_d / 1.6$) we get a daytime backscatter vertical profile in good agreement with the nighttime one (Figure S1b). A linear fit between the f_d / f_n and mean aerosol backscatter coefficient ($\beta = [\beta_n + \beta'_d] / 2$), results in the following relationship between the scaling factor (SF) and β

$$5 \quad SF = f_n / f_d = 1 / [0.123 + 0.148 \cdot \beta] \quad (3)$$

We combined equations (3) and (1) and get the estimate of nighttime equivalent data for the Arctic as shown in Fig. 3a–b. The monthly nighttime equivalent aerosol extinction coefficients agree with the nighttime one within 10% during winter (September–April). During May and July, the nighttime aerosol extinction is higher than the nighttime-equivalent one, as the nighttime overpass only reach up to 62°N and over 60% of the 60–62°N band is covered by continents and generally has higher
 10 aerosol extinction than the central Arctic. The wintertime (November–April) vertical profile of nighttime-equivalent aerosol extinction agrees with the nighttime one within 5% (Fig. S3b).

We also derive the nighttime-equivalent scaling factor for the Antarctic in the same manner (Fig. S2), and get:

$$SF = 1 / [0.121 + 0.122 \cdot \beta] \quad (4)$$

The calculated nighttime-equivalent aerosol extinctions in the Antarctic is in close agreement with the nighttime ones in
 15 February–November (Fig. S3c). The much higher nighttime aerosol extinction, in December–January, compared to the nighttime-equivalent, is again due to the limited nighttime overpass up to 62°S, and the zonal mean aerosol extinctions decrease toward south pole over the Southern Ocean (Fig. 3). The wintertime (May–October) nighttime equivalent vertical profiles closely agree with the nighttime data (Fig. S3d).

2 Calculating FYI and MYI in MERRA

20 The multi-year ~~(MYI)~~ sea ice (MYI) extent in this study is defined as the minimum sea ice extent during summer (September for Arctic and February in Antarctic) in the MERRA fields. In January–September over the Arctic, the MYI sea ice extent is the previous September minimum sea ice extent. We apply the same method for the Antarctic. We calculate the first-year sea ice (FYI) extent by subtracting the MYI extent from the MERRA total sea ice extent. Figure S4 shows the seasonal variations of FYI and MYI sea ice extent over the Arctic and Antarctic.

25

3 Monthly maps of aerosol extinction coefficients

Fig. S5 and S6 show 2007-2009 mean monthly maps of the distribution of aerosol extinction coefficients over the Arctic and Antarctic for November through April (Arctic) and May through October (Antarctic). Monthly extinction coefficients from CALIOP are compared to those from the four GEOS-Chem simulations. Also shown in Fig. S5 and S6 are monthly FYI and MYI sea ice coverage. Overall, the monthly comparisons are consistent with the mean cold-season comparison (Fig. 1 and 4 in the main manuscript), with STD+Opt. Snow best capturing the spatial distributions of CALIOP aerosol extinction coefficients among four model simulations

4 Sensitivity blowing snow simulations

We conduct two sensitivity simulations: 1) STD+Snow (N=1), which is the same as the STD+Snow simulation but assumes N=1 (number of SSA particle produced per snowflake) instead of N=5; 2) STD+Const. Snow, same as STD+Snow but applying a higher surface snow salinity on FYI over the Arctic (0.11 psu) and lower surface snow salinity on FYI over the Antarctic (0.018 psu). The choice of the FYI salinity was made to minimize the cold-months bias between GEOS-Chem and CALIOP. Results are shown in Fig. S7 for the Arctic and Fig. S8 for the Antarctic. Over the Arctic, the STD+Opt. Snow has best agreement with CALIOP among four blowing snow simulations. Over the Antarctic, the STD+Opt. Snow, STD+Snow (N=1) and STD+Const. Snow display similar model performances.

References

Di Pierro, M., Jaeglé, L., Eloranta, E. W., and Sharma, S.: Spatial and seasonal distribution of Arctic aerosols observed by the CALIOP satellite instrument (2006–2012), Atmos. Chem. Phys., 13, 7075-7095, <https://doi.org/10.5194/acp-13-7075-2013>, 2013.

Winker, D. M., Vaughan, M. A., Omar, A., Hu, Y., and Powell, J. A.: Overview of the CALIPSO Mission and CALIOP Data Processing Algorithms, J. Atmos. Ocean. Tech., 26, 2310–2323, doi:10.1175/2009JTECHA1281.1, 2009.

Arctic (62-70 N, 2007-2009)

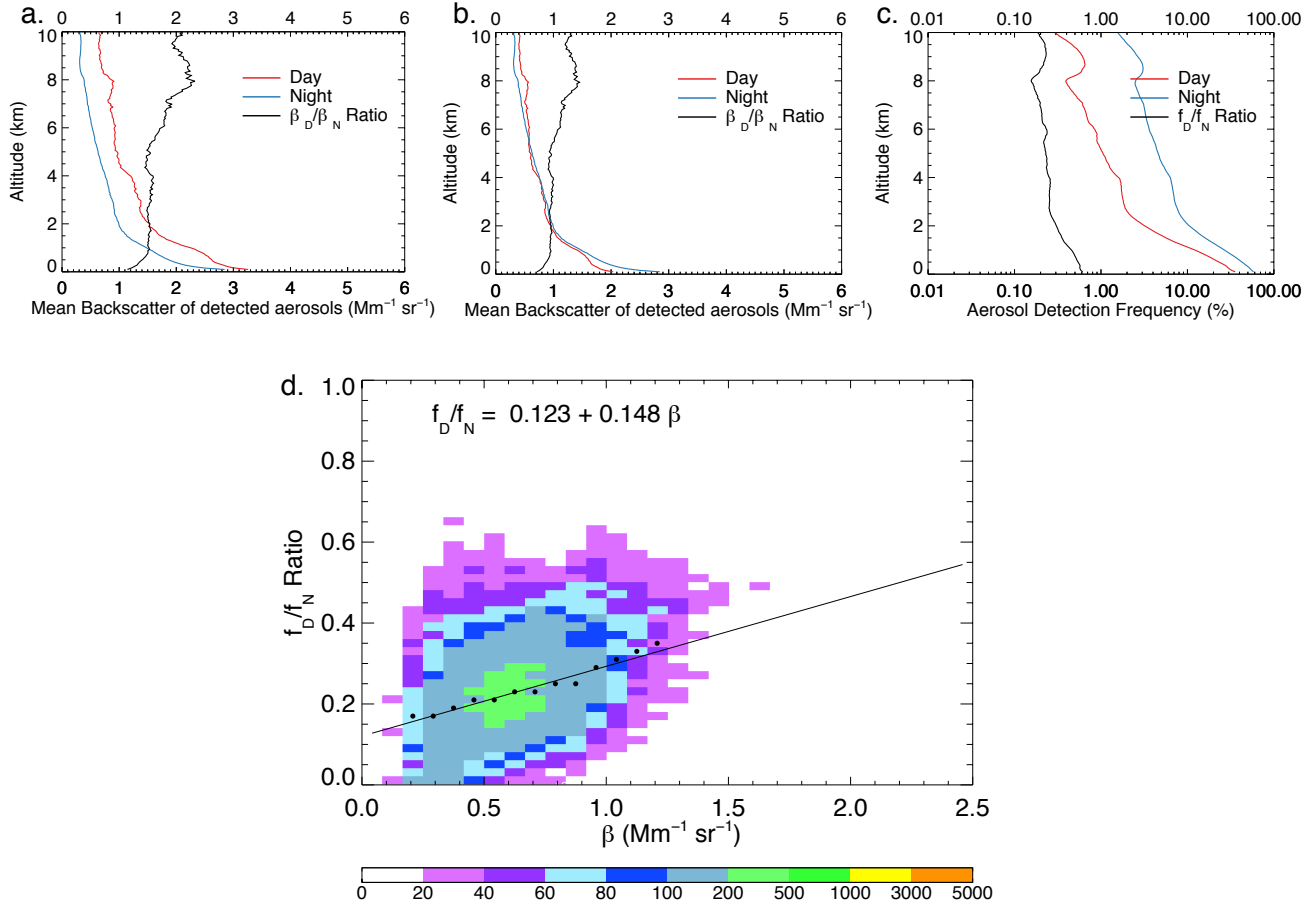


Figure S1: Vertical profiles of backscatter coefficients for detected aerosol layers (a–b) and aerosol detection frequency (c) in November–April 2007–2009 at 62°–70°N. The daytime backscatter coefficients shown in (b) are scaled ($\beta'_d = \beta_d/1.6$). Daytime profiles are shown in red lines, and nighttime profiles are shown in blue lines. The black lines in a–b indicate the ratios of daytime-to-nighttime backscatter coefficients. The black line in (c) shows the ratios of daytime-to-nighttime aerosol detection frequency (f_D/f_N). Shown in (d) is the scatterplot of f_D/f_N ratio as a function of the mean backscatter coefficients. The colors represent the number of points in each bin. Black circles are the median f_D/f_N ratio for the corresponding mean backscatter coefficient. The black line is the linear fit of the black circles.

Antarctic (62-70 S, 2007-2009)

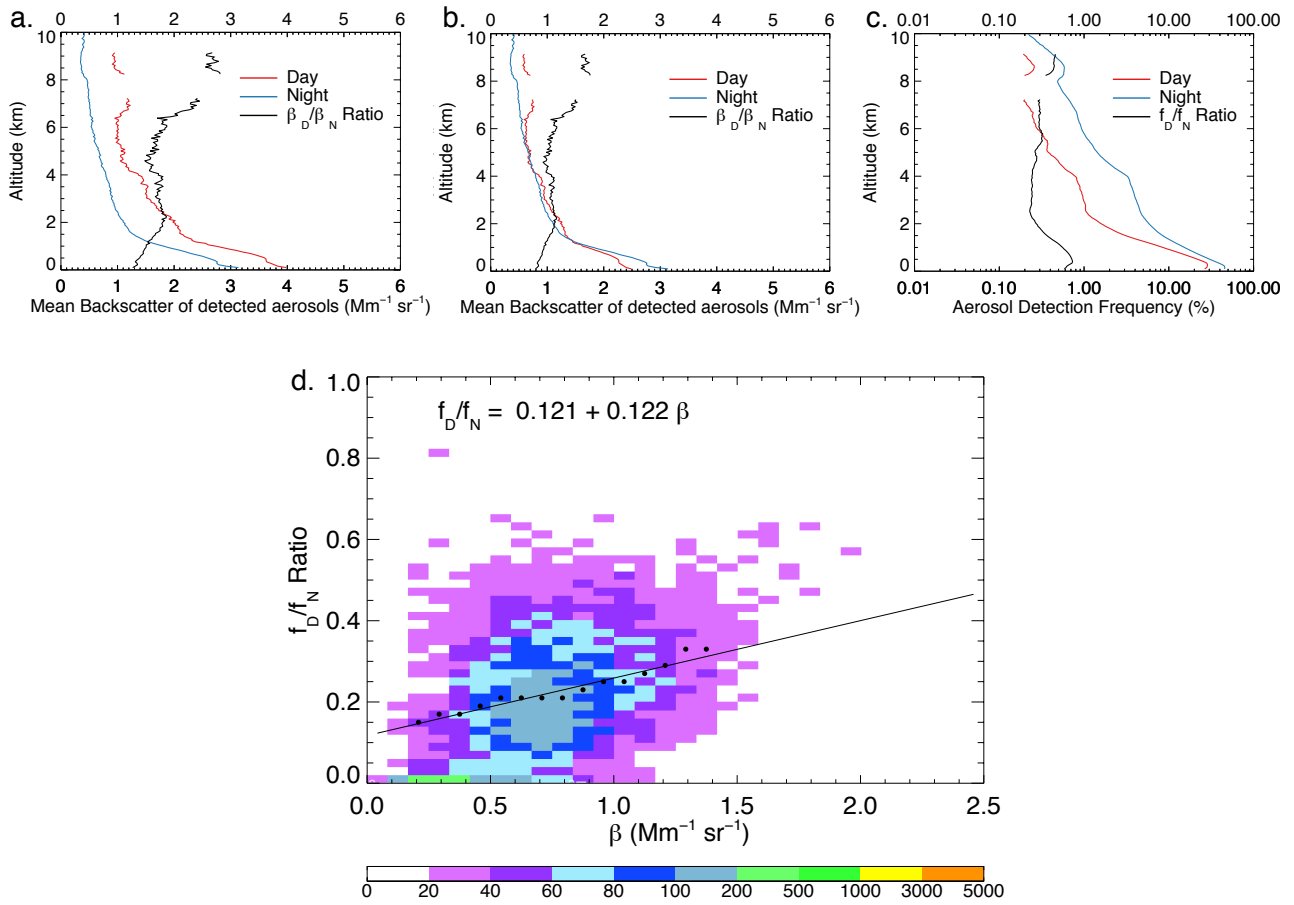
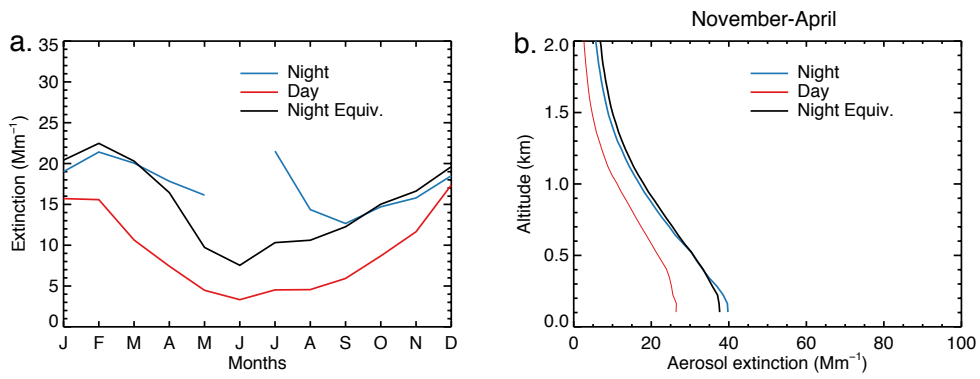


Figure S2: Same as Figure S1, but for May–October 2007–2009 at 62°–70°S.

Arctic (60-84 N, 2007-2009)



Antarctic (60-80 S, 2007-2009)

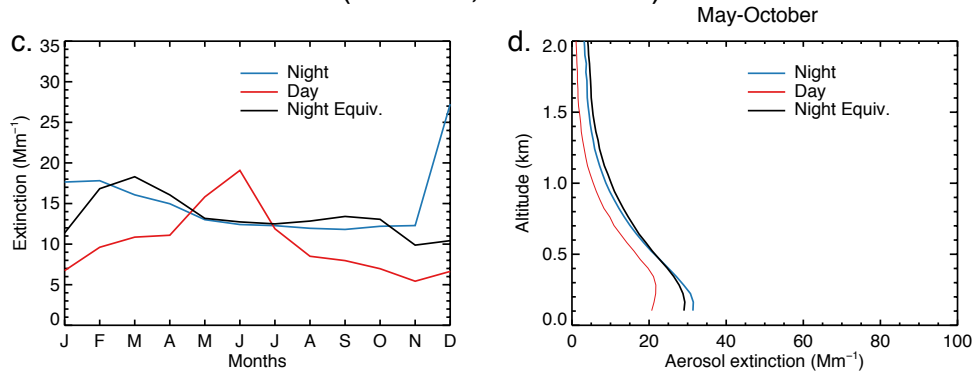


Figure S3: Comparison of seasonal variations of daytime, nighttime and nighttime-equivalent extinction coefficients over the (a) Arctic and (c) Antarctic. Also shown are the vertical profiles of daytime, nighttime and nighttime-equivalent extinction coefficients in the (b) Arctic winter (November–April) and (d) Antarctic winter (May–October).

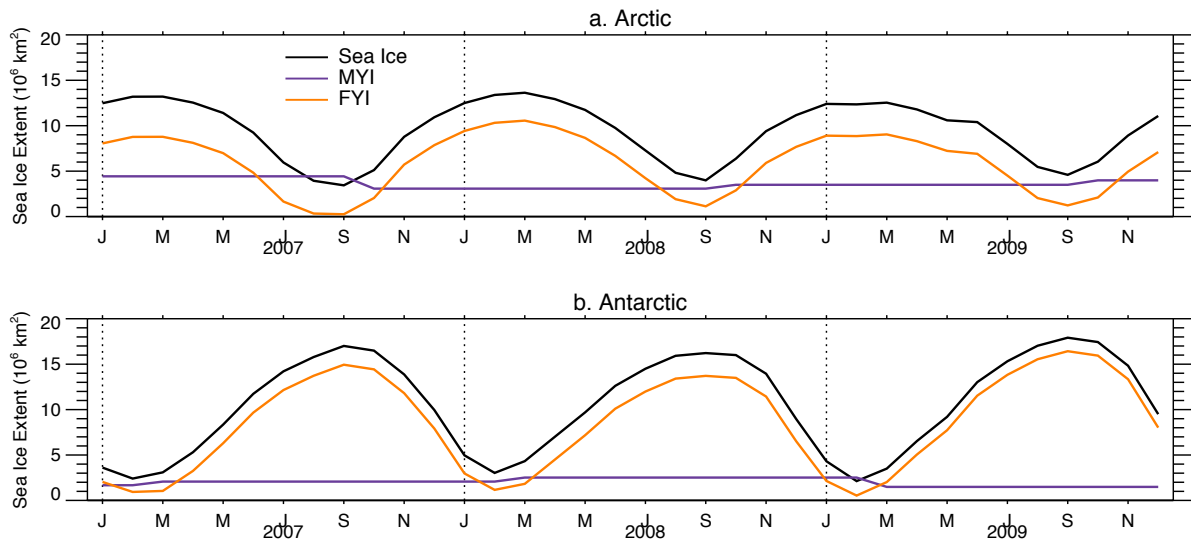


Figure S4: Seasonal variation of monthly sea ice extent (10^6 km^2) of total sea ice (black lines), first-year sea ice (FYI, orange lines) and multi-year sea ice (MYI, purple lines) over the (a) Arctic and (b) Antarctic.

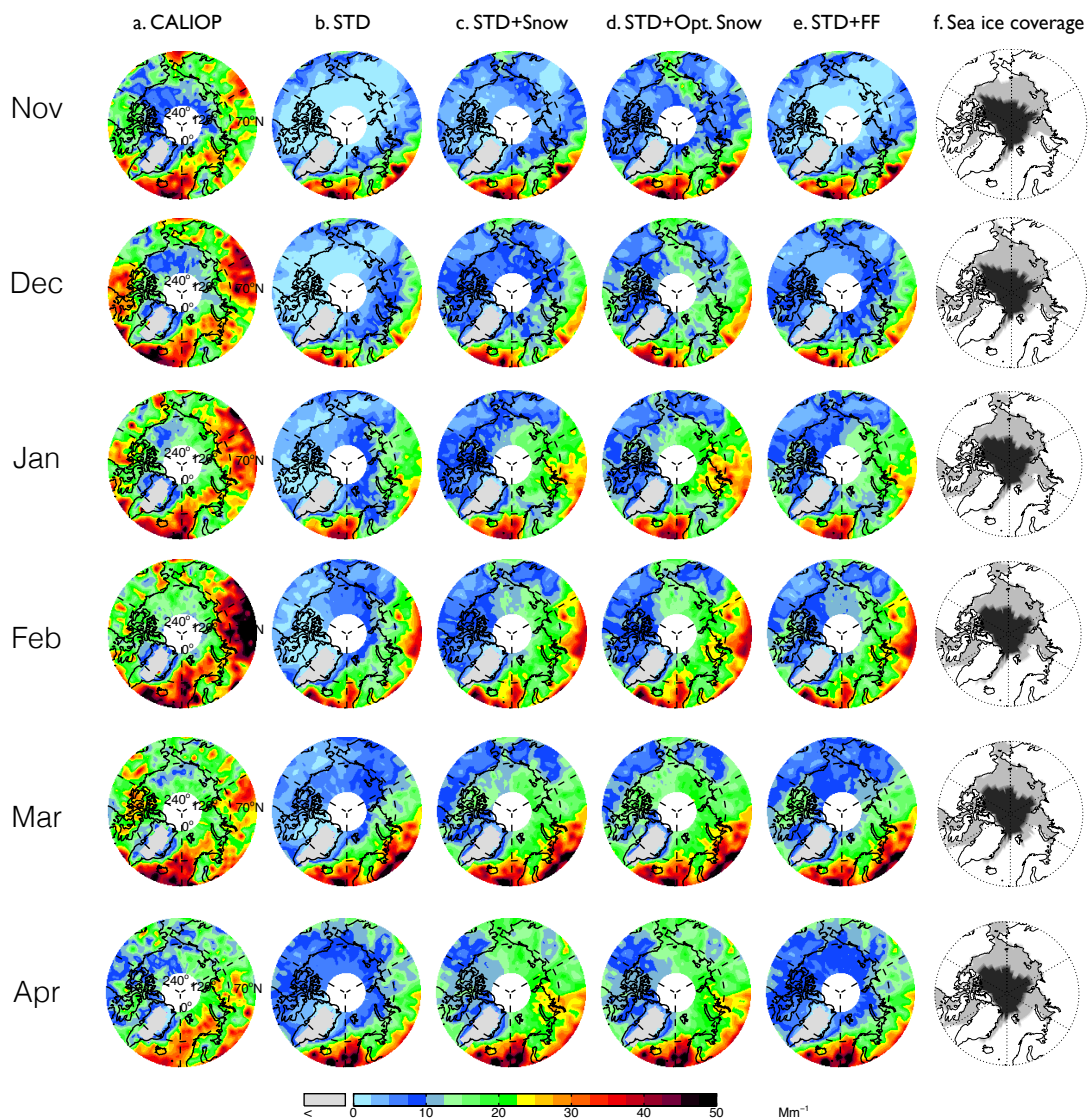


Figure S5: Monthly mean (2007-2009) spatial distribution of mean aerosol extinction coefficients (0–2 km) for November through April over the Arctic observed by (a) CALIOP and calculated with the GEOS-Chem model in (b) a Standard simulation (STD), (c) a simulation including blowing snow SSA emissions (STD+Snow), (d) an optimized blowing snow simulation (STD+Opt. Snow), and (e) a simulation including frost flower SSA emissions (STD+FF). The simulated extinctions are sampled at the time and location of the CALIOP overpasses, and the CALIOP sensitivity threshold is applied. Also shown are the (f) monthly MERRA sea ice coverage, with light gray shading indicating FYI and black shading for MYI.

5

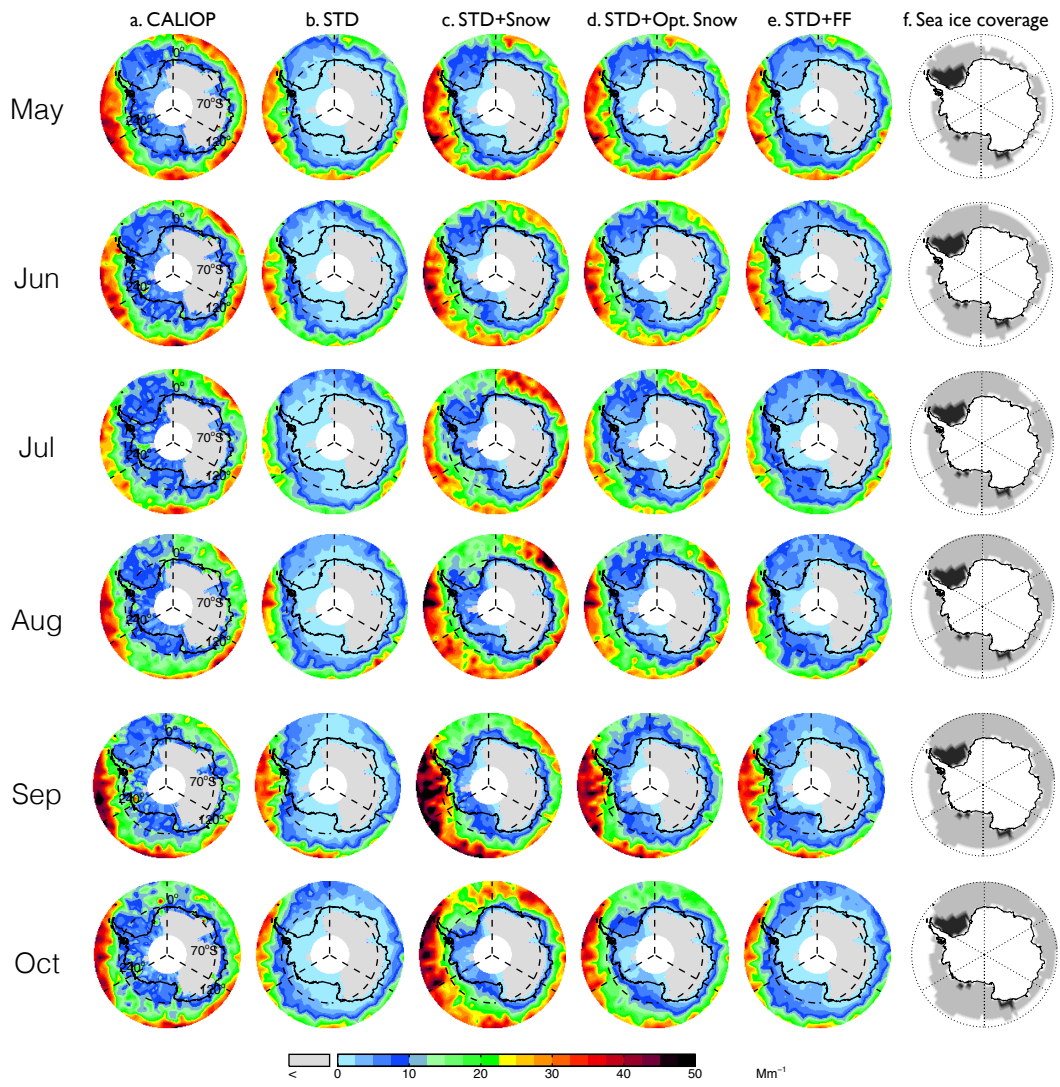


Figure S6: Same as Figure S5, but for Antarctic cold months (May–October)

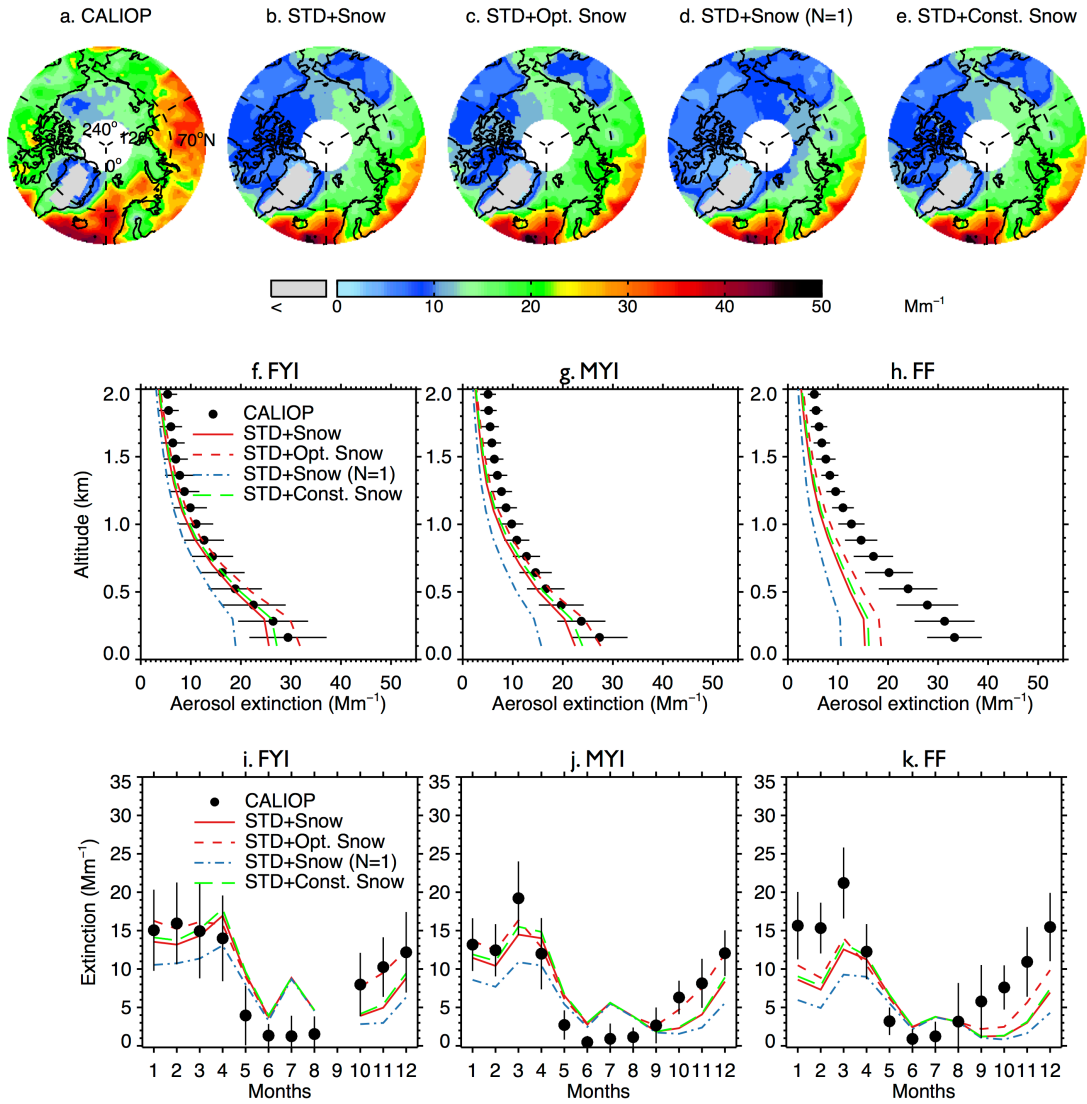


Figure S7: Cold season (November–April) spatial distribution of mean aerosol extinction coefficients (0–2 km) in the 2007–2009 over Arctic observed by (a) CALIOP and calculated with the GEOS-Chem model in (b) a simulation including blowing snow SSA emissions (STD+Snow), (c) an optimized blowing snow simulation (STD+Opt. Snow), (d) same as STD+Snow simulations but with number of particle produced per snowflake $N=1$ (STD+Snow ($N=1$)), and (e) same as STD+Snow simulations but applying a single scaling factor for surface snow salinity (STD+Const. Snow). Middle row: Vertical profiles of Arctic cold season mean aerosol extinction coefficients over (d) FYI, (e) MYI and (f) CAA for CALIOP (black dots with horizontal lines indicating standard deviations) and GEOS-Chem model simulations (STD+Snow: red solid lines, STD+Opt. Snow: red dashed lines; STD+Snow ($N=1$): blue dashed lines; STD+Const. Snow: green dashed lines). Bottom row: Seasonal cycle of 0–2 km monthly aerosol extinction coefficients averaged over (g) FYI, (h) MYI and (i) CAA. CALIOP observations are shown as black circles and vertical lines indicate the interannual standard deviation. The four GEOS-Chem model simulations are also shown (STD+Snow: red solid lines, STD+Opt. Snow: red dashed lines; STD+Snow ($N=1$): blue dashed lines; STD+Const. Snow: green dashed lines).

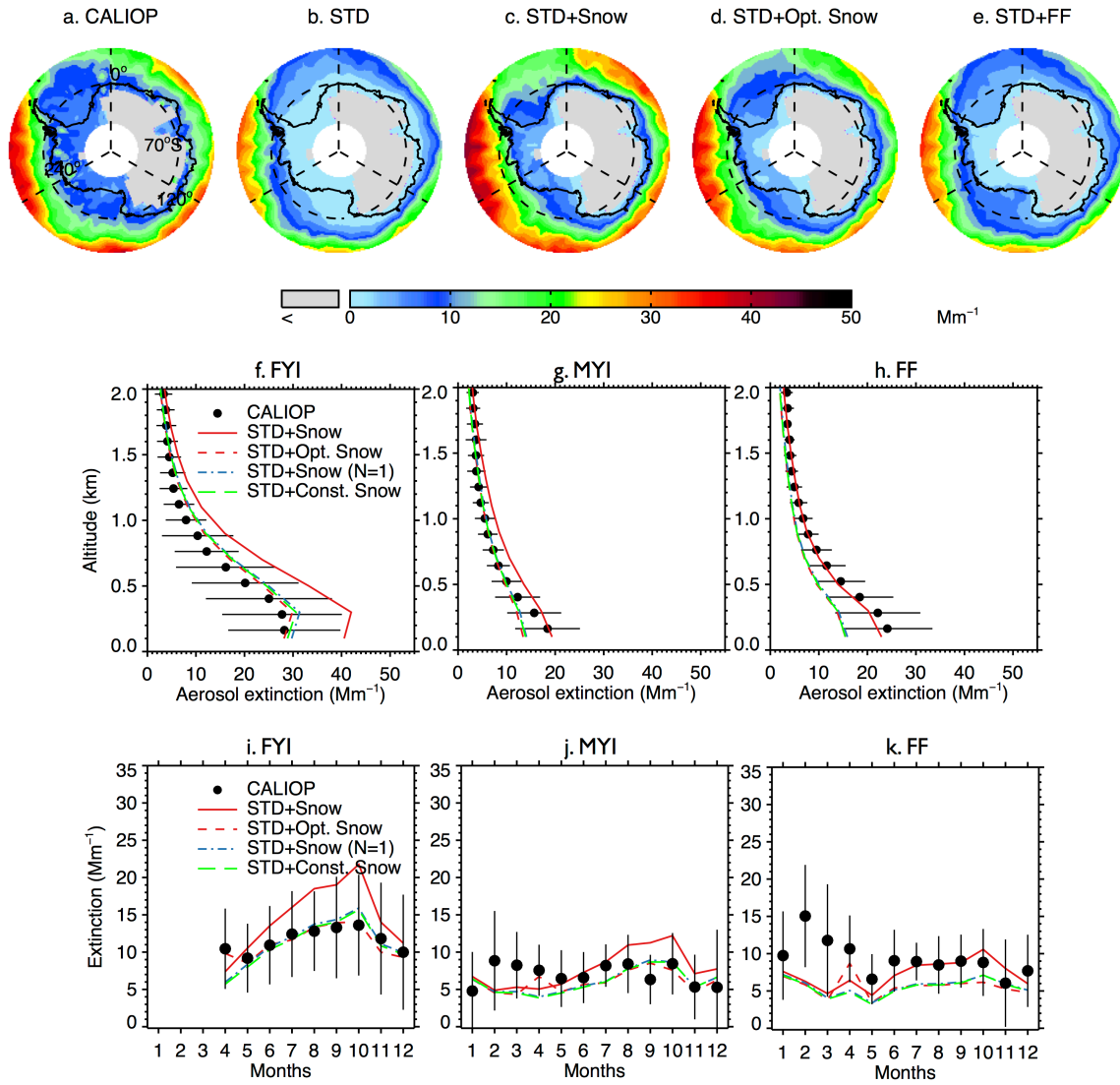


Figure S8: Same as Figure S7, but for the Antarctic aerosol extinction coefficients during Austral winter (May–October) over FYI (excluding offshore Ross Ice-shelf), MYI and offshore Ross Ice-shelf. As shown in (f), the monthly average aerosol extinction coefficients are not available over FYI during Antarctic summer (January–March) due to the limited FYI extent.